LATE CENOZOIC GEOLOGY OF SALAR BASIN, EASTERN SLOPE OF THE GRAND BANKS OF NEWFOUNDLAND

Michael W. Toews

Geological Survey of Canada Open File #1675

2003

Natural Resources Canada   Ressources naturelles Canada

Canada

GEOLOGICAL SURVEY OF CANADA

OPEN FILE #1675

Late Cenozoic geology of Salar Basin, eastern slope of the Grand Banks of Newfoundland

Michael W. Toews

2003

©Her Majesty the Queen in Right of Canada 2003
Available from
Geological Survey of Canada
Bedford Institute of Oceanography
1 Challenger Drive
Dartmouth, Nova Scotia B2Y 4A2

Toews, M.W.
2003: Late Cenozoic geology of Salar Basin, eastern slope of the Grand Banks of Newfoundland, Geological Survey of Canada, Open File 1675, 68 p.

Open files are products that have not gone through the GSC formal publication process.

ABSTRACT

This study describes the Cenozoic geologic framework of Salar basin, on the eastern slope of the Grand Banks, south of Flemish Pass. Data collected along the slope between 150 and 1700 m water depth include Huntec and single-channel airgun acoustic profiles, and four piston cores. Oligocene pelagic sediments at the base of a major unconformity display moating produced by a strong bottom current. An erosive scarp along the slope at 1.3 s TWTT indicates another period of strong bottom current. The scarp is overlain by a prodeltaic wedge, which developed around the late Pliocene to early Pleistocene. This also corresponds with the onset of turbidite deposition on the lower slope. Mass-transportation deposits and unconformities are recognized in the airgun and Huntec profiles, which occur at various magnitudes, and most events appear to occur episodically. Some failure events appear widespread throughout the study area, while others are geographically limited. Piston cores show the upper sediments consist of mud and ice-rafted detritus, and at least five Heinrich layers have been identified. Two or three intervals of glacial till totalling 60 m are interpreted to be stacked on the upper slope, which terminate between 450 and 500 m present water depth.

TABLE OF CONTENTS

LIST OF TABLES AND FIGURES

FIGURE (CONTINUED) **PAGE**

1.0 INTRODUCTION

The study area is located in the northern part of Salar basin, on the continental slope east of the Grand Banks of Newfoundland (Figs. 1, 2). The sediments deposited in the area during the Late Cenozoic are dominantly terrigenous mud and ice rafted deposits. Ice-sheets extended across the Grand Banks in the Late Quaternary, and terminated in the study area. Ice-proximal sediments on the Canadian Atlantic margin accumulate and prograde rapidly and are susceptible to slope failures (Piper & Sparkes, 1987; Piper, 1988; Mosher et al., 1989; Pickrill et al., 2001). Little is currently known about the Late Cenozoic geology in the area, and although preliminary, this report attempts to describe the geologic framework. Particular interests are the sedimentary structures revealed by high-resolution seismic profiles, slope instability hazards, and the influence of ice-sheets and icebergs on the sedimentary environment.

Data used in this study was collected by the Geological Survey of Canada (Atlantic) during two cruises (99031, 2001043) and includes Huntec DTS (deep-tow seismic) sparker and airgun acoustic profiles, and several piston cores (Sonnichsen, 1999; Piper, 2001). The data were collected along the continental slope between 150 and 1700 m water depth.

1.1 GEOLOGIC SETTING

Salar basin is the name given to the structurally-controlled basin which formed as the North Atlantic Ocean rifted open in the Late Triassic to Early Jurassic (Austin et al., 1989; Enachescu, 1992). It is also known as the outer Carson basin, since a basement high separates it from Carson basin proper. The 20,000 km^2 Salar basin depocenter is filled with evaporites, carbonates and clastic deposits, and is oriented parallel to the southeast edge of the Grand Banks between Flemish Cap and the Southeast Newfoundland Ridge. Continental ice-sheets extended across the Grand Banks in the Late Pleistocene, and terminated in the study area at their glacial maximum during the

Wisconsinan glaciation (Piper & Campbell, in press).

1.2 REGIONAL PHYSIOGRAPHIC SETTING

The study area (Figs. 1, 2) is bounded by Carson Canyon to the southwest, and Flemish Pass to the northeast. Insular Newfoundland is 400 km to the west. Regional bathymetric contours show that the slope has an irregular morphology, but it is not as incised by canyons as the slope off the southern Grand Banks. The shelf break is at about 150 m, but it has a rather rounded morphology compared with other areas of the Grand Banks (Fig. 1). The slope flattens out to a terrace at 1400 m, before descending to the abyssal plain. Larger gullies and small canyons appear below the 1400 m isobath. The continental slope drainage system diverts into two directions downslope from the study area: part is directed eastward into an unnamed canyon which continues south of Flemish Cap, while the remainder continues southeast towards the Newfoundland basin near the Newfoundland Seamounts.

2.0 METHODS

This study uses data acquired during CCGS Hudson cruises 2001043 and 99031 (conducted in the summers of 2001 and 1999). Acoustic data collected during these cruises include Huntec sparker, single-channel airgun, 12 kHz and 3.5 kHz sounder profiles. Additionally, sidescan sonar data were acquired for shallow water depths during the 99031 cruise. In total, over 300 line km of data were collected. Bathymetric data were obtained from 12 kHz sounder reflection paper profiles.

Huntec DTS sparker data were interpreted using paper copies and have a vertical resolution of about 0.3 m and acoustic penetration of 0.1 s (75 m). Sediments appearing in these records are typically soft and geologically young, and for simplicity can be assumed to have a constant P-wave velocity of about 1500 m/s; about the same as seawater. This velocity approximation is supported by the physical property measurements from the piston cores.

Piston cores from both cruises (Table 1) can be tied in with seismic lines, and were obtained using the AGC long piston corer. Trigger weight cores were recovered for most of the cores, except 027. Prior to be being split, the cores were logged using a multi-sensor track, to obtain continuous physical property logs of magnetic susceptibility, P-wave velocity, and bulk density by gamma-ray attenuation. The cores were photographed and described using standard core lab procedures. A continuous digital colour log was obtained using a spectrophotometer, and the results are displayed in L*a*b* format. Shear strength was measured in the 2001043 piston cores using a mini-shear vane device. A radiocarbon date result has been returned for core 001, while two shell samples from the 2001043 cores are awaiting results at the time of writing. A few X-ray diffraction (XRD) samples from cores 001 and 030 have been analyzed to determine the carbonate/terrigenous ratio for intervals suspected of being Heinrich layers. The carbonate/terrigenous ratio is calculated by identifying peak areas for calcite, dolomite, illite (10 Å), kaolinite + chlorite (7 Å) and quartz and is often calculated by (cal+dol)/(illite+7A°+qtz). All of core 030 has been sampled at 5 to 25 cm intervals for carbon content using a LECO WR-112 carbon analyzer. Total carbon is found by combusting a 0.25 g ground sample from the core with lead and copper at ~1200°C. The carbon dioxide gas from the combustion is analyzed to determine the percent total carbon. Organic carbon is found similarly, except the sample is treated with hydrochloric acid for 24 hours prior to combustion to remove inorganic carbon (carbonate). Inorganic carbon is calculated from the difference between total and organic carbon.

High-resolution single-channel reflection data were obtained using two 0.65 L sleeve-airguns and a Benthos 100’ eel, and the digitized traces were recorded directly to Exabyte data tapes. The airgun profiles were interpreted digitally using The Kingdom Suite seismic analysis software. The 99031 survey has a dominant frequency of 160 Hz and an acoustic penetration of 0.6 s. The 2001043 survey has a dominant frequency of 120 Hz, and an acoustic penetration of 1.5 s.

3.0 RESULTS

3.1 BATHYMETRY PROFILES

Fig. 3 shows dip profiles of the 12 kHz bathymetry at locations indicated in Fig. 2. There are two distinctive ‘breaks’ in the dip profiles indicated by B1 and B2, as summarized in Table 2. The depths of inflexion point B1 ranges from 435 to 500 m and B2 from 960 to 1200 m. Both breaks tend to occur in deeper water to the north.

The slope is divided into upper, middle and lower slope sections. The gradients are derived from the regional bathymetry map (Fig. 2). The upper slope is above B1 and has a regional gradient of 1.5° above the 300 m isobath increasing to 4° at 500 m. The middle slope is from B1 (500 m) to about 1300 m. The steep section below B1 varies between 5-14° whereas the rest of the middle slope has a gradient of 3-5°. The lower slope is relatively flat in some areas, and as steep as 15° in other areas. The gradients can be higher in gullies and other local surficial features.

3.2 SIDESCAN RECORDS

A band of megaripples and parallel bedforms (Fig. 4) have been identified on the upper slope by Sonnichsen et al. (1999) between 120 and 165 m water depth, with crests oriented at 30 degrees and spaced 18 m.

3.3 HUNTEC PROFILES

Four seismic facies were recognized through the Huntec profile interpretation. However, not all profiles can be assigned to these facies.

For this report, mass movement processes including slumps, slides, and debris flows have been grouped together into mass-transport deposits. Mass-transport deposits (MTDs) are recognized throughout the study area. They appear in Huntec reflection profiles as a chaotic to transparent interval with a hummocky top, and an erosive base (e.g. Piper et al., 1985; 1999). Overlying reflections are commonly draped above the MTD.

3.3.1 FACIES CLASSIFICATION

The *till facies* is the only facies present on the upper slope (Fig. 5). It is found from the shallowest water depth records to ~500 m (B1). The acoustic signature is very distinctive and is characterized by a high-amplitude seafloor return, with incoherent internal reflections. It appears that the upper 5 ms are parallel continuous reflections, however this is likely ‘ringing’ from the high acoustic impedance contrast between the seawater and the seafloor. The surface is flat, though there are a few minor irregularities, which appear as scours (or pits) of only a few meters (up to 5 ms) deep and several tens of meters in width, and can have small raised berms on either side. In some areas, acoustic energy has returned from about 60 ms sub-bottom (Fig. 5) producing small isolated or grouped hyperbolic reflections. These reflections are weak and are not found throughout all of the profiles on the upper slope.

There are two facies on the middle slope, and can be easily identified by their surface character. A *hummocky middle slope facies* is usually found below B1 on steep parts of the slope (Fig. 6). The seabed surface is very irregular with many hyperbolic reflections. This is also the appearance in the 12 kHz bathymetric profiles, though a true profile would have sharper bathymetric features with steeper gradients. The internal reflections of the hummocky deposits are incoherent to chaotic, and resemble MTDs, but in water depths of <700 m these could also be a result of iceberg turbation. Sediment may have been deposited in some depressions, as evidenced by parallel reflection packages. Reflections below the hummocky deposits are sub-parallel to parallel and discontinuous, and cannot be correlated with other reflections in the study area. Downslope, these underlying reflections also appear to be disrupted at lower stratigraphic intervals.

The *smooth/scarped middle slope facies* (Fig. 7) has a smooth surface with failure scarps and unconformities. The unconformities are usually angular on steep sections, but become paraconformable on more gently sloping sections. Internal reflections are typically parallel to sub-parallel and are continuous to discontinuous. These resemble the reflections found below the hummocky deposits in the previous facies. MTDs are uncommon in this facies, though a few shallow isolated MTDs have been identified.

Three facies are defined on the lower slope. The *smooth lower slope facies* (Fig. 8) is similar to the *smooth middle slope facies*, except it has shallow dipping or horizontal reflections, and fewer unconformities. Reflections are often parallel and continuous. Stacked and buried MTDs are found in some areas, resulting in the *smooth lower slope facies with stacked incoherent intervals* (Fig. 9). The *lower slope steep facies*, which is acoustically similar to the *smooth/scarped middle slope facies*, often occurs on short steep seafloor segments that have angular unconformities.

3.3.2 CORRELATIONS

Correlation of Huntec reflections was difficult and could not be done continuously over the entire area. The entire slope is dissected by escarpments, and has steep sections, making continuous acoustic ties impossible. Many correlations of key Huntec reflections are based on acoustic character. Reflections have been correlated across the lower slope with a reasonable amount of confidence using a combination of the ridges (Figs. 10, 11) for the deeper reflections, and flat lying reflections (Fig. 8) for the upper 0.04 s of reflections. These are summarized in Table 3. The type-sections cannot confidently be tied into reflections in the middle slope, although an attempt is made in Fig. 7 by acoustic character, using the same colouring scheme. The type section was defined in the 2001043 Huntec records, which are difficult to tie in with the lower quality 99031 records. Other correlations based on acoustic character at similar water depths in the study area (Figs. 8, 9) imply that very similar facies have developed at certain water depths and that correlations can be made between the two.

MTDs and associated unconformities have been identified over the study area, and their stratigraphic positions, indicated by letters *a* to *g*, are shown in Fig. 8 for the shallow stratigraphy, and in Figs. 10 & 11 for the deeper stratigraphy. Event *a* is characterized as a widespread unconformity usually found on steep slope sections at 2.5 ms sub-bottom depth. However, few corresponding MTDs have been found elsewhere at this stratigraphic level. Horizon *b* has MTDs and unconformities and is found principally in the southwest of the study area. Even *c* is the most widespread regional shallow MTD at 13 to 15 ms sub-bottom and is recognized in stacked MTD sections (Fig. 9). Event *d* has MTDs mainly in the northeastern part of the study area. Events *e*, *f* and *g* are unclear, as the data quality at this depth does not allow for confident correlations of reflection character. Event *e* is thought to be a major unconformity, limited to some areas of the slope, which in places eroded down to events *f* (Fig. 10) or even to *g* (Fig. 8). Event *g* is a major sediment failure event found throughout the study area, and is recognized in the airgun profiles. The event horizon *f/g* has either an angular unconformity (Figs. 10, 11) or is a hummocky reflection with incoherent underlying reflections (Fig. 8).

3.3.3 MORPHOLOGY

Several ridge or mounded seismic facies have been found in the Huntec records (Figs. 10, 11), which are considered to be part of the *smooth lower slope facies*, with *lower slope steep facies* on either side. These consist of sequences of draped parallel reflections with angular unconformities (illustrated as thin red lines on Figs. 10, 11) cutting down through the sides. The gradients of reflections in the ridges also increase upsection. The adjacent gullies contain slumped deposits (chaotic reflections, on the right side of Fig. 10) and stacked MTDs (left side of Fig. 10; Fig. 11).

The stratigraphic positions of the unconformities in each of the ridges are nearly identical. Some unconformity horizons have symmetrically cut down on both sides of the ridge, while others appear to drape conformably on one side, while cutting down on the other (asymmetric erosion). It is unknown whether all of the unconformities have had sediment eroded off the middle of the ridge, although correlation of certain stratigraphic intervals in each of the figures indicates that some stratigraphic intervals are missing (represented by a red rectangle). The distance between the two illustrated ridges is 6 km. These unconformities may be episodic, with an interval of ~5 ms and the last (uppermost) event occurring 2.5 ms sub-bottom.

3.4 CORE DATA

Cores obtained in the study area (Table 1, Fig. 12) generally have dark grey/brown mud with ice rafted deposits, and Heinrich intervals (H0 to H6?). Ice rafted detritus is generally coarse sand to gravel size, though some clasts are nearly as large as the core width (~10 cm).

Heinrich events are episodic times of rapid iceberg calving from the Hudson Strait and other icesheet outlets. The discharged icebergs passed through the Labrador Sea and the Newfoundland margin, leaving beds of detrital carbonate, called Heinrich layers (Andrews & Tedesco, 1992). The ages of the layers are well known from radiocarbon and other dating studies (e.g. Bond & Lotti, 1995) and provide a useful chronology of the sediment sequences found in the piston cores. The last (uppermost) Heinrich layer, numbered H0, marks the beginning of the Holocene. The layers associated with the last (Wisconsinan) glaciation are numbered from H1 to H6.

The trigger-weight cores (Appendix A), which accompany the piston cores (except for 027, which was not recovered), indicate that little sediment is missing from the top of the piston cores during coring, so that the depth in the core and the real depth from the seabottom are approximately the same.

Piston core 001 is from the deepest water in the study area, and is situated on a slight gradient on the lower slope. Huntec profiles around the core site indicate that there may be an unconformity with associated MTDs at about 10 ms or 750 cm depth, although this is not evident in the core. The core consists dominantly of mud with abundant granules and some shell fragments. Analysis of the carbonate/terrigenous ratio (Appendix A) confirms the presence of H0 at 240 cm, suggested by slightly elevated L* and bulk density values. A radiocarbon date confirms H1 at 551 cm depth.

Piston core 027 is from the shallowest water, below the steep section downslope of B1 on the *smooth middle slope facies*. It consists of winnowed sand (some intervals are well sorted) and mud with abundant clasts ranging from granules to cobbles. Two Heinrich layers are recognized in this core, and a radiocarbon date is expected to confirm the age of the upper layer as H1. This core is short, probably because the corer was stopped by a large clast.

Piston core 028 was collected on a steeply inclined slope with several angular unconformities through the core, according to the Huntec records (Fig. 7). The uppermost unconformity in the Huntec data occurs at 2.5 ms or 1.9 m (Fig. 7, 2001-043 data), and the second is at 4 ms or 3 m depth (1999-031 data). The upper half of the core is dominantly muddy sand, while the lower half is dominantly sandy mud. The shear strength significantly changes at 115 cm, which may indicate an unconformity. This piston core has a MTD within the upper meter, and a shell extracted below this MTD is awaiting a radiocarbon age that will provide a maximum age for the MTD and confirm the age of the uppermost Heinrich layer.

Piston core 030 is from a relatively flat area in the lower slope, which according to the Huntec records does not have any unconformities or MTDs within the depth of the core. The core consists dominantly of mud with some granules and dropstones, and a few sand intervals. This core provides an excellent chronology of sedimentation in the lower slope, with at least five Heinrich layers, defined by the total carbon curves. (Note that the organic and inorganic carbon determinants are incorrect, due to incomplete digestion of carbonate). A thin H0 layer is found at 30 cm sub-bottom, and is supported by the high carbonate/terrigenous ratios from the XRD data.

3.5 AIRGUN PROFILES

Interpreted reflection profiles are displayed in Figs. 13 to 18, and their locations are in Fig. 2. All scales between the figures are constant. Uninterpreted profiles are available in Appendix B. The quality of the 99031 data is poor, since the digital recording window was not optimally configured in some parts of the profiles.

3.5.1 KEY REFLECTIONS

The type section for the key reflectors for the upper and middle slope are defined from the 2001043 survey in B-B′ (Table 4, Fig. 14), and the order and attributes of the reflection horizons are summarized in Table 4. Correlations of reflections between the middle and lower slope are tentative, since there are no reliable continuous reflections connecting the two, and no wells have been drilled in either area. The acoustic signatures in the airgun profiles appear to change along the upper and middle slope, which makes correlation difficult, especially since the seismic surveys zigzag up and down the slope.

The green reflection is an angular unconformity, separating underlying rocks of Jurassic and Cretaceous age (Grant et al., 1988; Grant & McAlpine; 1990; Enachescu, 1992) from the Cenozoic rocks relevant in this study. The profile of the unconformity is remarkably similar to that of a typical passive margin shelf profile, with a sharp shelf break defined by a basement high. It is this buried basement high that separates Salar basin from Carson basin (Enachescu, 1992), or the inner Carson basin from the outer Carson basin (Grant et al., 1988). The Lower Cenozoic shelf break has depths of 1.4 s in A-A′, 1.7 s in B-B′, 2.0 s in C-C′, and 1.9 s in D-D′. Furthermore the Lower Cenozoic shelf break is seaward of the modern shelf break in all the profiles, except for A-A′, and has formed the shape of the terrace outlined by the 1400 m isobath (Fig. 2). The green unconformity typically has a high amplitude reflection, is underlain either by incoherent reflections or folded/parallel reflections. The contact is angular in several profiles.

The package of reflections above the green unconformity are of low amplitude and are sub-parallel. On the lower slope, they onlap the unconformity surface, whereas on the upper middle slope they are sub-parallel to the unconformity surface. A few strong reflections are traced though this package in the figures as magenta, yellow and pink. Reflections at the foot of the green unconformity surface downslope from the basement high are undulatory (A-A´, B-B´ and C-C´; Figs. 13, 14, 16), and may be a result from moating by bottom currents. Moating is a decreased or non-deposition or even erosion of sediments which lie at the base of a slope due to high velocity bottom slope currents, which flow along isobaths (McCave & Tucholke, 1986). In profile A-A´ (Fig. 13) the package of sediments above the green unconformity is slightly sigmoidal, and is much thicker than in the other profiles.

The seismic facies above yellow have higher amplitudes and are slightly more parallel, although moating is still apparent in some places along the base of the slope. Dark blue is an unconformity found in the middle and lower slope, and has a profile similar to the present day slope profile, and is heavily scarped into the slope at 1.3 s. It is overlain by another unconformity, orange, which is distinctive in the upper slope of A-A´ and B-B´ (Figs. 13, 14) as a high amplitude reflection. This orange unconformity horizon is the basis for transferring reflections from the middle slope to the lower slope and vice versa, particularly in C-C´ (Fig. 16). The reflections above orange also have high amplitudes, and are downlapping and prograding seaward on the upper and middle slope. Here, the reflections 0.15 s above orange in profiles A-A´ and B-B´ (Figs. 13, 14) show the strongest progradation and form a wedge on the orange horizon. The seismic facies between brown and orange is rather incoherent in places, and changes thickness, it is therefore the top of the deepest major regional MTD recognized in the profiles. Other reflections above orange are slope parallel, and converge on the middle slope to inflexion point B2.

Cyan marks an unconformity surface that has developed gullies in B´-C´, and shows considerable gully and small canyon development in D-D´. The purple reflection is correlated from middle to lower slopes based on comparisons of sediment thicknesses, on the acoustic character, and on its position relative to the orange reflection. On the upper surface, it is the base of a package of parallel high amplitude reflections, which continue down the middle slope with loss of amplitude strength. On the middle slope of profiles A-A′ and B-B′ (Figs. 13, 14) the purple horizon is overlain by an incoherent and hummocky facies surface, which is the hummocky middle slope facies from the Huntec records (Fig. 6). This facies is associated with erosion; therefore some of the purple horizon may be incorrectly traced where it does not exist. The light-purple horizon is considered part of the same seismic facies as purple, except it can only be correlated through the upper slope. It is parallel to the purple reflection, and is only used to mark a strong reflection below the incoherent facies on the upper slope. On the lower slope, the purple reflection marks an unconformity, which has shaped gullies that extend to the cyan horizon. This unconformity is found in all of the profiles. The small canyon in D-D′ is further incised by the purple reflection, and is filled with an incoherent seismic facies. Continuous reflections onlap the gullied depressions. Above the purple horizon on the lower slope there appears to be a few unconformity horizons and incoherent/hummocky intervals, which suggest sediment failure events, however these horizons are difficult to distinguish and correlate due to their scale.

The unconformity surface labeled *f/g* (Figs. 8, 10, 11) in the Huntec profiles has been transposed into the airgun profiles, and is traced as a red horizon. This surface has similar characteristics to the major unconformity recognized in the Huntec profiles, since it can be angular and can have an underlying incoherent interval. Above the red horizon, there are several other unconformities and MTD facies, however they are best resolved using the Huntec data.

3.5.2 UPPER SLOPE PROFILES

Fig. 19 shows airgun profiles through the end of the ice-sheet moraine deposits on the upper slope. The light-purple reflection (Fig. 19) is a high-amplitude continuous reflection on the upper slope, and is parallel to the purple horizon (Figs. 13, 14, 16-18), which correlates downslope. The light-purple and purple reflections appear to be contained in a single high-amplitude acoustic unit. Above this unit are parallel medium amplitude reflections, which thicken downslope. The tan horizon is an irregular surface, which steps through the underlying reflections, implying that it is an erosional unconformity. Above tan, a few continuous and discontinuous reflections are present, however the upper 0.12 s of the airgun profile are incoherent reflections with what appear to be discontinuous reflections. The incoherent reflections are interpreted as till, while the discontinuous reflections (blue) are interpreted as stratified material (using reasoning outlined by Piper et al., 2002). The identifiable of the discontinuous blue horizons are tentative, however they coincide with the isolated weak hyperbolic reflections in the Huntec records (Fig. 5). The profiles are interpreted to have two or three units of the incoherent facies (till) in the upper slope. In Fig. 19 A, B, E the incoherent till reflections terminate at 0.6-0.7 s below sea level (indicated by the orange dash), and in Fig. 19 D reflections through the material appear to laterally pass from incoherent to continuous reflections facies at the same depth. The maximum depth of the till deposits appear to be constantly offset from the inflexion point B1 by 0.07 s in all the profiles.

4.0 DISCUSSION

In Flemish Pass, along strike to the north, exploratory wells and regional petroleum-industry seismic-reflection profiles show that lower Oligocene to Quaternary sediments overlie two major stratigraphic units recognized by Kennard et al. (1990), bounded by unconformities, and overlying folded Mesozoic rocks. They assigned ages based on correlation with wells in the region. Unit 1 is characterized by low-amplitude, discontinuous, chaotic reflections overlain by parallel to sub-parallel undulating reflections interpreted as sediment drift, whereas Unit 2 exhibits remarkably smooth parallel bedding that illustrates the southward migration of the axis of Sackville Spur through time. The base of Unit 1, forming sediment drift features, was correlated with a middle Oligocene unconformity in the Gabriel C-60 well and the base of Unit 2 with a middle Miocene to early Pliocene unconformity in the same well. Kennard et al. (1990) suggested that this unconformity at the base of Unit 2 may correlate with the regional "Merlin" unconformity on the US Atlantic margin (Mountain & Tucholke, 1985) that resulted from intensification of bottom current circulation in the late Miocene. Alternatively, the sedimentation above the basal unconformity in unit 2 may not have begun until the late Pliocene, when in the Labrador Sea bottom circulation decreased in intensity and sedimentation rate increased substantially (Srivastava et al., 1987; Myers & Piper, 1988). This interpretation is supported by correlation of a late Pliocene biostratigraphic pick in borehole 88-400-06 on the Grand Banks to near the base of Unit 2 (Piper & Pereira, 1992).

The Oligocene to Cretaceous unconformity in Flemish Pass resembles the green unconformity illustrated at the western end of line B-B′ (Fig. 14). Although such correlation along strike remains speculative, the moating in the green reflector at the eastern end of line B-B′ supports the interpretation that the green reflector is Oligocene or younger. The character of the dark blue reflector on the upper slope is similar to the Unit 1/Unit 2 unconformity at a similar water depth in Flemish Pass and is therefore tentatively interpreted as on late Miocene to late Pliocene age.

The green reflection in the airgun profiles defines a shelf to slope profile from the Early Cenozoic, with the shelf break at the seaward margin of the basement high and significant erosion on the slope.

The sediments between the green unconformity and the dark blue unconformity are interpreted to be uniform clay to silt sized pelagic sediments. These have onlapped the green unconformity surface. Moating at the base of the slope (e.g. yellow horizon in Fig. 14) is from deep Labrador Current activity, which first flowed strongly in the

Oligocene (McCave & Tucholke, 1986). In profile A-A′, there is a thick package of sediments between green and dark blue, in contrast to B-B′, and this may be due in part to transportation of sediments along contours from bottom current activity. The blue unconformity is probably current related, with a maximum erosion scar at 1.3 s.

The orange horizon marks a change in acoustic facies in the study area, whereby overlying reflections are sharper and more continuous in the lower slope. This acoustic change is observed on the Scotian margin at the mid-Pliocene boundary (Piper & Normark, 1989), and may mark a shift in sedimentation style on the lower slope to include turbidite deposition. The downlapping reflections above orange on the upper and middle slope in profiles A-A′ and B-B′ could be prograding deltaic sediments. This acoustic characteristic is less obvious or absent in the other profiles. During glacial periods of the Quaternary, the Grand Banks were emergent, and rivers crossed the banks with glacial meltwater from insular Newfoundland. Above orange on the middle and lower slope appears to be the oldest regional MTD recognized in the airgun data (brown). This MTD above orange is probably associated with the prograded sediments, and may have occurred at different times. Other reflections above orange are well-stratified prograded sediments, which converge on the middle slope towards B2. This could be due to the influence of a deep Labrador Current at 1100-1300 m below the present sea level.

Cyan is a horizon that shows the first development of gullies in the study area, and is best seen in the oblique dip profile D-D′ (Fig. 17). It is also closely related with purple, which also has more erosion over the study area. Both of these events might be associated with one or more lowstands.

The high-amplitude acoustic unit on the upper slope (bounded by purple and light-purple) is interpreted as interbedded mud and sand produced from winnowing by strong isobath-following currents. This type of sediment facies can have a high-amplitude seismic signature, for example on the upper slope near the Storegga Slide off Norway. The reflections appear to have the strongest amplitudes between 0.5 and 0.9 s in the profiles, which could be related to water depths of the winnowed sand package. This unit is interpreted as preglacial sediments, since neither glacial till nor the draped signature of proglacial muds are recognized at the stratigraphic level.

Reflections above light-purple have lower amplitudes, and are more irregular, which suggest a dominance of mud. The tan horizon on the upper slope is an irregular unconformity that resembles a stepped failure plane. Fig. 19 A is an oblique dip line through the upper slope, and may have captured cross-sections through retrogressive slump horizons. Such retrogressive slumps in proglacial mud in places fail down to the preglacial sediments, which have a higher shear strength. The water depth and profile of the tan horizon is remarkably similar to seabed profiles found on the St. Pierre slope after the 1929 Grand Banks earthquake failures (Piper et al., 1999).

There are at least two or three units of till on the upper slope. They appear to be separated by highly discontinuous stratified sediments. The till and stratified sediments are in total about 60 m thick, and the maximum depth is 0.07 s below B1. As an ice-sheet first advanced into the study area, it would have traveled across soft preglacial sediments, which would have been easily eroded and perhaps deformed. The depth and degree which the base of the ice-sheet could erode would be controlled according to many factors, of which two are sea level and ice thickness. The wedge of stratified proglacial sediments which appear to thicken with depth is where the ice-sheet started to floated off from the underlying sediments. During subsequent retreats and advances of the ice, stratified sediments would be deposited in front of the ice-sheet, and eroded in much the same manner. Irregularities of the discontinuous reflection surfaces (blue) in the incoherent till reflections could be anything from meltwater channels to push-moraines during readvances, and may be discontinuous due to total erosion of stratified material during an ice-sheet readvance.

There are only small iceberg scours and pits on the seabottom of the upper slope, which may indicate there is not much other sediment on top of the till blanket, since till has a high resistance to deformation. Megaripples in 150 m water depth (Fig. 4) indicate that sand locally overlies the till. The megaripples are created by currents flowing northeast (along the isobaths) either during storm events and/or from the Labrador Current.

The seabed appears to be mildly scoured and iceberg turbated in some areas (Fig. 3) between 500 and 620 m water depth, consistent with the maximum depth of iceberg scouring in Flemish Pass of 700 m reported by Piper & Pereira (1992).

One explanation of the first slope break, B1, is where stratified proglacial sediments have retrogressively failed back to the till, as seen on the Scotian Slope (Pickrill et al., 2001). Downslope from B1, sediment was totally removed on the steep slope in Figs. 12 A, B, E. However, in Fig. 12 D it appears there are slump blocks downslope of B1, with later iceberg turbation. The timing of such failure events is unknown in this area. Huntec profiles with the *hummocky middle slope facies* below the iceberg turbation limit (Fig. 6) are interpreted to be a result from such a failure as described. However, the morphology and development of the *hummocky middle slope facies* remains uncertain.

The depth at which the inflection point B1 occurs, interpreted to be directly related to the limit of till deposition, increases from about 450 m in the south to 500 m in the north of the study area. The simplest interpretation of this trend is that glacial ice was thicker in the north. In Flemish Pass to the north, the limit of till deposition is obscured by iceberg scouring, but may correspond to the change in iceberg scour pattern at 510 m. (Piper & Pereira, 1992).

The entire slope in the study area below B1 appears to be susceptible to slope instability hazards, and many unconformities and failure scarps have been identified. Based on the Huntec reflection profiles, these failure events can occur episodically and remove material from the middle slope to deeper water. Four types of failure events have produced unconformities and MTDs:

(1) Horizons *g* and *h* (or red in the airgun profiles) mark widespread failure events, which have produced large angular unconformities and/or MTDs. The deposit under the brown horizon in the airgun profiles appears to be similar, except that it is thicker.

(2) Several medium-sized failure events have been found in the Huntec records, which erode material from steep slopes, and deposit the material in the lower slope, often in stacked MTDs. These MTDs appear in the same stratigraphic position over great distances on the lower slope (Fig. 9), and lead to the development of the *smooth lower slope facies with stacked incoherent intervals*.

(3) Small scale failure events occur on steep slopes, such as on the ridges. The correlations of the unconformities in Huntec profiles in Figs. 10 & 11 suggest that the triggering of the events are synchronized, despite the distance between the two ridges. These events occur episodically, as shown by the semi-regular spacing between events.

(4) Isolated MTDs are found in a few areas (Fig. 8) that do no tie in with other MTDs.

Failure event types 1-3 suggest a regional trigger, such as an earthquake or melting of gas hydrate with fall in sea level. In contrast, failure event type 4 is triggered from isolated sources, such as an iceberg disturbing unstable sediments on a steep slope.

The Huntec profiles of the ridges on the lower slope (Figs. 10, 11) show the morphology of gullies. The steepening of reflections upsection could be related to the maturation of the ridges with time. The ridges consist principally of proglacial muds deposited in a draped manner from surface plumes (Piper & Sparks, 1987), whereas the gullies are maintained by erosive flow of turbidity currents. Sediments in Fig. 11 appear to have started slumping at the brown horizon, and have stopped at about 3 ms sub-bottom.

The inferred failures in the Salar basin are similar to those found on the Scotian Slope, where the availability of multibeam bathymetry, more seismic reflection profiles and cores makes interpretation more reliable (Pickrill et al., 2001). In both areas, upper slope till marks an abrupt break in slope and much of the middle slope below the till limit appears to have failed. Failures are common on the flanks of canyons on the Scotian Slope and are then draped by younger proglacial sediment, as is seen on the flanks of gullies in Salar basin. Complete evacuation of sediment along bedding planes is common on both the Scotian Slope and the Salar basin.

Cores taken from the area show a general trend of finer material at deeper water depths, and coarser material in ice-proximal shallower water depths. These cores also have a higher amount of IRD than in cores from the Scotian margin in similar water depths. This is due to a large flux of icebergs through the area, which follow the Labrador Current. The Labrador Current presently has a strong influence on sedimentation in the vicinity of core 027 in 651 m water depth, since its uppermost sediments are sorted sand.

The piston cores provide an estimate of sedimentation rates and hence a means of applying a chronology to the slope sediments. This discussion of chronology is tentative until the ages in the cores are confirmed by additional radiocarbon dating. However, the identification of Heinrich event H3 in cores 001 and 030 suggests sedimentation rates of 0.25 to 0.35 m/ka at 1300 to 1700 m water depth. This implies an age for horizon *f* of 90 - 150 ka: over this interval, about ten failure surfaces are recognized in Figs. 10 & 11.

6.0 RECOMMENDATIONS

The available data are not sufficient to make accurate and confident correlations of Huntec and airgun reflections across the study area. More high quality Huntec and airgun profiles need to be done across the area. Strike seismic profiles across the lower and middle slopes would be useful in ensuring good correlations across the area, since the existing survey profiles zigzag up and down the slope across areas where reflections are difficult to continuously correlate. There are only a few piston cores in this area, and more are required to understand the sedimentation rates and chronology of events found in the stratigraphy and acoustic profiles. Interesting places to collect cores would be near where the airgun reflections converge to near B2, since it appears to have remarkably compressed stratigraphy; and cores in the areas with similar acoustic stratigraphy (Figs. 7, 8), to compare if the lithology is also similar.

High-resolution bathymetry (multibeam or reprocessed 3D surface renders) on the Scotian Slope has proven to be very useful in studying the regional seabed morphology (Pickrill et al., 2001). Such data over the study area would be useful for studying the surficial and Quaternary geology. High-resolution bathymetry would help indicate the texture and geometry of such seabed features. It could also be combined with other data to map re-occurring failure scarps and surficial deposits. Iceberg scours and turbation zones could also be identified. Future expeditions can benefit from this imagery since Huntec lines and piston cores can be strategically placed in areas of interest.

6.0 CONCLUSIONS

This study has provided a regional geological model for the late Cenozoic sediments of the Eastern Grand Banks Slope between Carson Canyon and southern Flemish Pass. In the Late Tertiary, the region appears to have had a similar water depth to the present and to have accumulated hemipelagic sediment under the influence of the southward-flowing Labrador Current. The onset of turbidite sedimentation in deep water corresponds to the development of a prodeltaic wedge on the upper slope, probably in the late Pliocene and early Pleistocene. This succession is overlain by several stacked till sheets on the upper slope, that have prograded across and pass downslope into proglacial muds. The limit of these tills, at 450 - 500 m, is marked by an abrupt increase in slope, as a result of failure of muds on the middle slope.

From relatively little data, this geological model provides a framework for assessing geotechnical properties and slope stability seabed sediment. Principal geohazards are related to slope instability ice-proximal deposits. Slope failures appear more abundant than in comparable areas of the Scotian Slope. Coarse ice-rafted detritus is more abundant than on the Scotian Slope and might locally be concentrated. No evidence has been seen in the limited data set for shallow gas or gas hydrate.

ACKNOWLEDGEMENTS

This work was done during a Cooperative Education work term. The writer wishes to express his thanks to David Piper for continuous support and patience in this project. Gratitude is also expressed to Calvin Campbell, Gary Sonnichsen, Chris Jauer, Dave Mosher and many other people at the Geological Survey of Canada (Atlantic) for their support. This work was funded by the Program for Energy R & D project 532211.

7.0 REFERENCES

Andrews, J.T., and Tedesco, K., 1992. Detrital carbonate-rich sediments, northwestern Labrador Sea: implications for ice-sheet dynamics and iceberg rafting (Heinrich) events in the north Atlantic. Geology, **20**, 1087-1090.

Austin, J.A., Tucholke, B.E., and Uchupi, E., 1989. Upper Triassic–Lower Jurassic salt basin southeast of the Grand Banks. Earth and Planetary Science Letters, **92**, 357-370.

Bond, G.C., and Lotti, R., 1995. Iceberg discharges into the North Atlantic on millennial time scales during the last glaciation. Science, **267**, 1005-1010.

Enachescu, M.E., 1992. Enigmatic basins offshore Newfoundland. Canadian Journal of Exploration Geophysics, **28**, 44-61.

Grant, A.C., Jansa, L.F., McAlpine, K.D., and Edwards, A., 1988. Mesozoic-Cenozoic geology of the eastern margin of the Grand Banks and its relation to Galicia Bank. In: Proceedings of the Ocean Drilling Program, Scientific results, Galicia margin ; covering Leg 103 of the cruises of the drilling vessel JOIDES Resolution, Ponta Delgada, Azores, to Bremerhaven, Germany, 25 April 1985-19 June 1985. Edited by: Mazzullo, E.K. Proceedings of the Ocean Drilling Program, Scientific Results, **103**, 787-808.

Grant, A.C., and McAlpine, K.D., 1990. The continental margin around Newfoundland. In: Geology of the Continental Margin of Eastern Canada. Edited by: Keen, M.J., and Williams, G.L. Geological Survey of Canada, Geology of Canada, No. 2, 239-292.

Kennard, L., Schafer, C., and Carter, L., 1990. Late Cenozoic evolution of Sackville Spur: a sediment drift on the Newfoundland continental slope. Canadian Journal of Earth Sciences, **28**, 863-878.

Mountain, G.S., and Tucholke, B.E., 1985. Mesozoic and Cenozoic geology of the U.S. Atlantic continental slope and rise. In: Geologic evolution of the United States Atlantic margin. Edited by: Poag, C.W. Van Nostrand Reinhold, New York, 293-342.

McCave, I.N., and Tucholke, B.E., 1986. Deep current-controlled sedimentation in the western North Atlantic. In: The Geology of North America, Vol. M, The Western North Atlantic Region. Edited by: Vogt, P.R., and Tucholke, B.E. The Geological Society of America, 451-468.

Mosher, D.C., Piper, D.J.W., Vilks, G.V., Aksu, A.E., and Fader, G. B., 1989. Evidence for Wisconsinan glaciations in the Verril Canyon area, Scotian Slope. Quaternary Research, **31**, 27-40.

Myers, R.A., and Piper, D.J.W., 1988. Seismic stratigraphy of late Cenozoic sediments in the northern Labrador Sea: a history of bottom circulation and glaciation. Canadian Journal of Earth Sciences, **25**, 2059-2074.

Pickrill, R., Piper, D.J.W., Collins, J., and Gee, L., 2001. Scotian Slope Mapping Project: The benefits of an integrated regional high-resolution multibeam survey. Offshore Technology Conference, OTC 12995, Houston, Texas, 30 April–3 May 2001.

Piper, D.J.W., 1988. DNAG Glaciomarine sedimentation on the continental slope of Eastern Canada. Geoscience Canada, **15**, 23-28.

Piper, D.J.W., 2001. Cruise Report: Hudson 2001-043. Geological Survey of Canada (Atlantic), internal report.

Piper, D.J.W., and Campbell, D.C., 2002. Quaternary geology of Flemish Pass and its application to geohazard evaluation for hydrocarbon development. Geological Association of Canada, paper in press.

Piper, D.J.W., Cochonat, P., and Morrison, M.L., 1999. Sidescan sonar evidence for progressive evolution of submarine failure into a turbidity current: the 1929 Grand Banks event. Sedimentology, **46**, 79-97.

Piper, D.J.W., Farre, J.A., and Shor, A.N. 1985. Late Quaternary slumps and debris flows on the Scotian Slope. Geological Society of America Bulletin, **96**, 1508-1517.

Piper, D.J.W., Mosher, D.C., and Newton, S., 2002. Ice-margin seismic stratigraphy of the central Scotian Slope. Current Research, Summer 2002.

Piper, D.J.W, and Normark, W.R., 1989. Late Cenozoic sea-level changes and the onset of glaciation: impact on continental slope progradation off eastern Canada. Marine & Petroleum Geology, **6**, 336-347.

Piper, D.J.W., and Pereira, C.G.P., 1992. Late Quaternary sedimentation in Flemish Pass. Canadian Journal of Earth Sciences, **29**, 535-550.

Piper, D.J.W., and Sparkes, R., 1987. Proglacial sediment instability features on the Scotian Slope at 63°W. Marine Geology, **76**, 15-31.

Sonnichsen, G.V., King, E.L., MacLean, B., 1999. CSS Hudson 99-031: a seabed survey of northern Grand Bank and Flemish Pass. Geological Survey of Canada (Atlantic), internal report.

Srivastava, S. P., Arthur, M.A. et al., 1987. Sites 645-647 Baffin Bay and Labrador Sea: Proceedings of the Ocean Drilling Program, part A, v. 105.

Station No.	Latitude	Longitude	Water Depth (m)	Core Length (cm)	No. of Sections	TWC* Length (cm)
99031						
001	45.390955	-47.960671	1690	1078	7	165
2001043						
027	45.673375	-47.970203	651	273	2	0
028	45.716446	-47.855831	1061	890	6	18
030	45.669488	-47.625900	1324	979	7	80

Table 1. Locations and specifications of piston cores.

* a trigger weight core (TWC) is essentially a gravity core that is independent from the piston core, but is extracted at the same time. This is used to help calibrate the piston core depth relative to the undisturbed seafloor.

Profile	Water Depth (m)	
	B1	**B2**
A	498	1205
B	*480*	*1155*
C	-	970**
D	462	1050
E	435*	960**

Table 2. Water depths of slope profile breaks.

* Calculated from Fig. 12E since 12 kHz bathymetry profiles do not extend to B1.

** Positions of breaks are unclear.

Type section for upper 0.04 m at 2001043 225/0704 (Fig. 8)

horizon	reflection attribute
a	low amplitude parallel reflection, below parallel high-amplitude package
flesh	parallel reflection at base of parallel low-amplitude package
b	high-amplitude parallel reflection
c	parallel reflection
pink	parallel reflection
purple	very high-amplitude doublet
d	low-amplitude parallel reflection
green	parallel high-amplitude doublet
yellow	reflection at top of parallel high-amplitude package
e	not well developed, possible unconformity, some chaotic and discontinuous reflections
brown (dashed)	not well developed (approximate correlation from Fig. 10)
f	angular unconformity down to *g*
g	angular unconformity overlaying hummocky incoherent reflections

Type section for lower reflections at 2001043 225/0605 (Fig. 10)

horizon	reflection attribute
a	low amplitude unconformity, below parallel high-amplitude package
b	unconformity down to *c*
c	angular unconformity
pink	parallel reflection
purple	high-amplitude reflection
d	angular unconformity
green	parallel high-amplitude doublet
yellow	reflection at top of parallel high-amplitude package
e	angular unconformity
orange	parallel high-amplitude reflection
teal	parallel high-amplitude doublet
brown	top of parallel high-amplitude reflection package
f	angular unconformity
blue	parallel high-amplitude doublet
g	high-amplitude angular unconformity

Table 3. Reflection horizons in Huntec records.

Type section in B-B´ (Fig. 14)

horizon	reflection attribute	interpretation
blue	discontinuous weak reflections	discontinuous stratified material enclosed in the till
tan	angular unconformity, stepping through intervals	unconformity through proglacial muds below the till
light-purple	parallel high-amplitude continuous reflection	preglacial winnowed sand and mud on upper slope
purple	parallel high-amplitude reflection on upper/middle slope; high-high amplitude angular unconformity on lower	preglacial winnowed sand and mud on upper/middle slope; base of gullies on lower slope
cyan	angular unconformity	base of some gullies and small canyons on lower slope
brown	top of incoherent reflections above orange	top of lowermost major regional MTD
orange	high-amplitude doublet angular unconformity overlain by some high amplitude reflections on upper/middle slope; high amplitude reflection overlain by high amplitude reflections on lower slope.	base of deltaic sediments on the upper/middle slope; base of turbidite deposition on lower slope
dark blue	angular unconformity on middle and lower slope	unconformity produced by strong current activity
pink	base of parallel reflection package above low-amplitude reflection package	reflection through pelagic sediments on lower slope
yellow	parallel reflection doublet through low-amplitude reflections	same as above
magenta	same as above	same as above
green	varied-amplitude angular unconformity	major Lower Cretaceous unconformity

Table 4. Reflection horizons in airgun records.

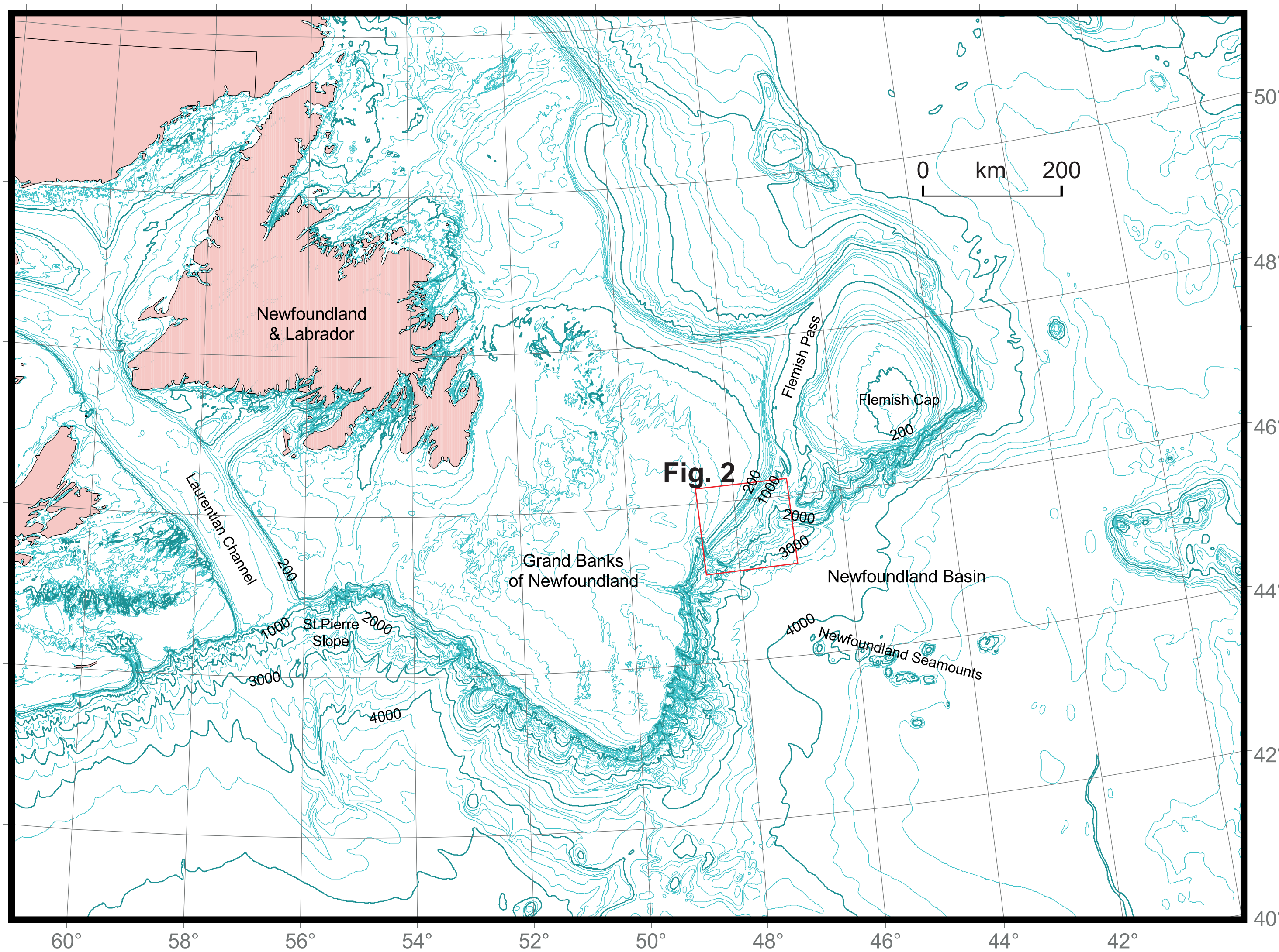

Figure 1. Bathymetric map of the continental margin off Newfoundland.

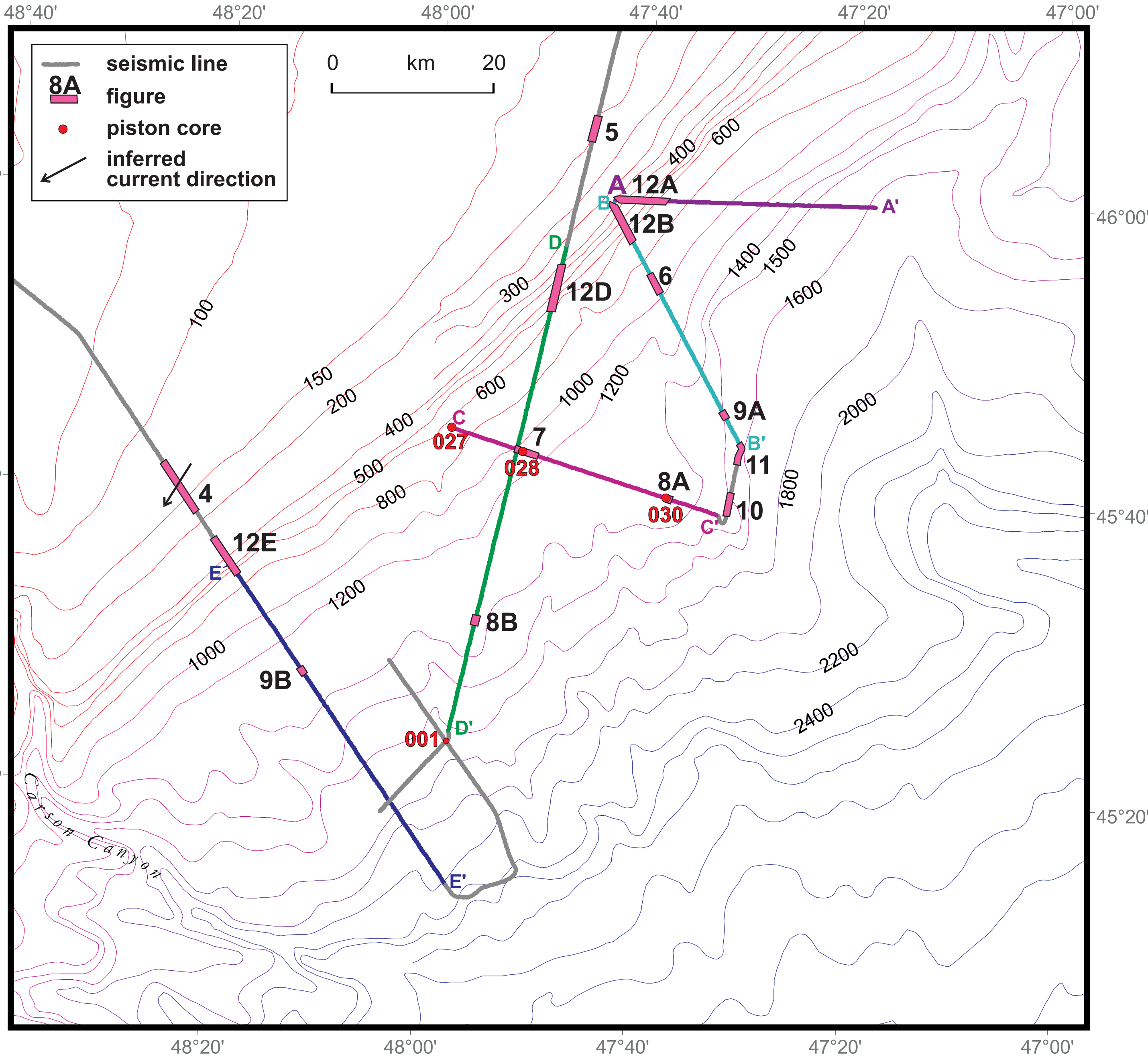

Figure 2. Study area with regional bathymetric contours, seismic lines, core locations, and figure locations. A-A´, B-B´, C-C'; D-D´ and E-E´ are dip profiles shown in Fig. 3, and are airgun seismic lines shown in Figs. 13-18.

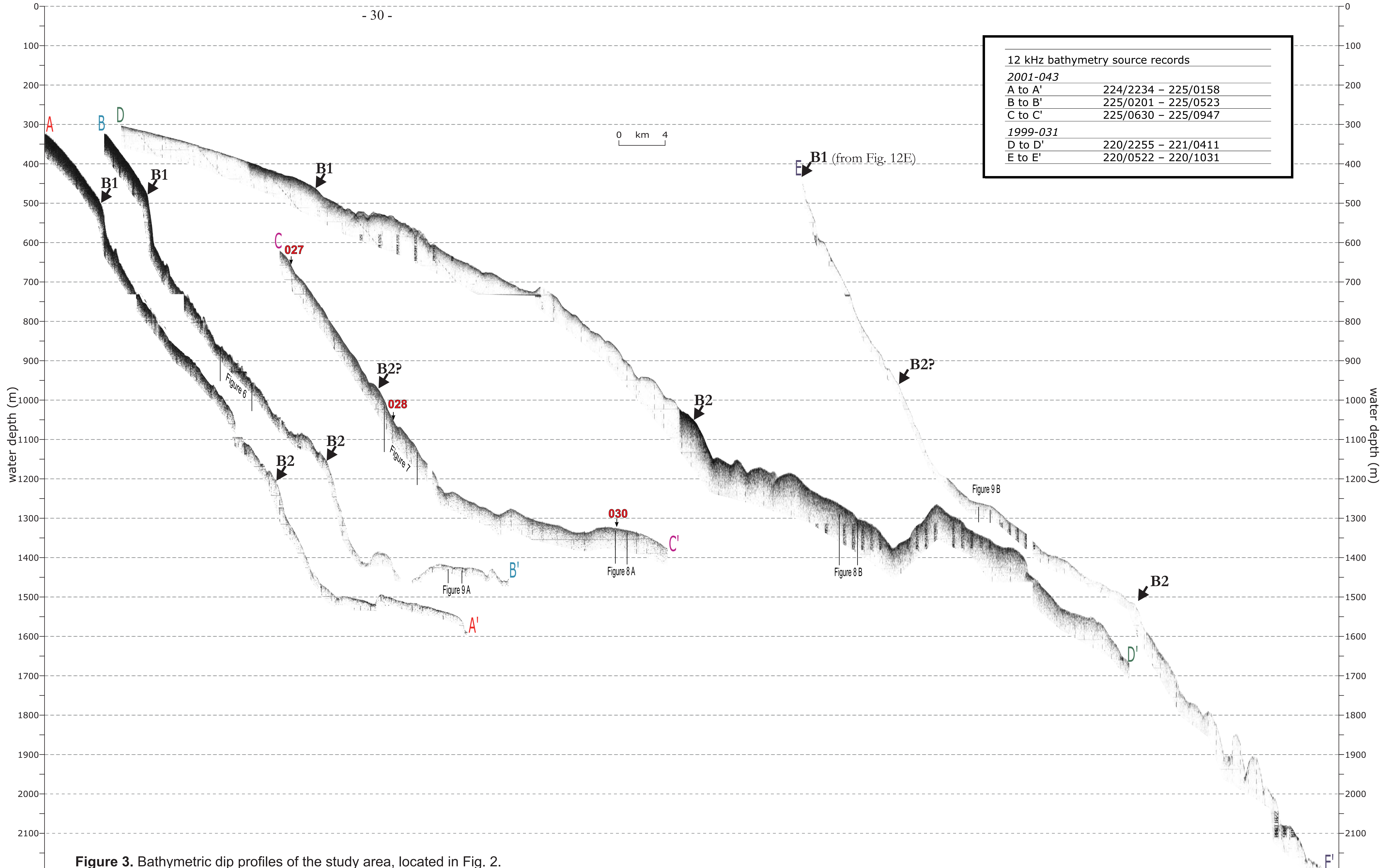

Figure 3. Bathymetric dip profiles of the study area, located in Fig. 2.

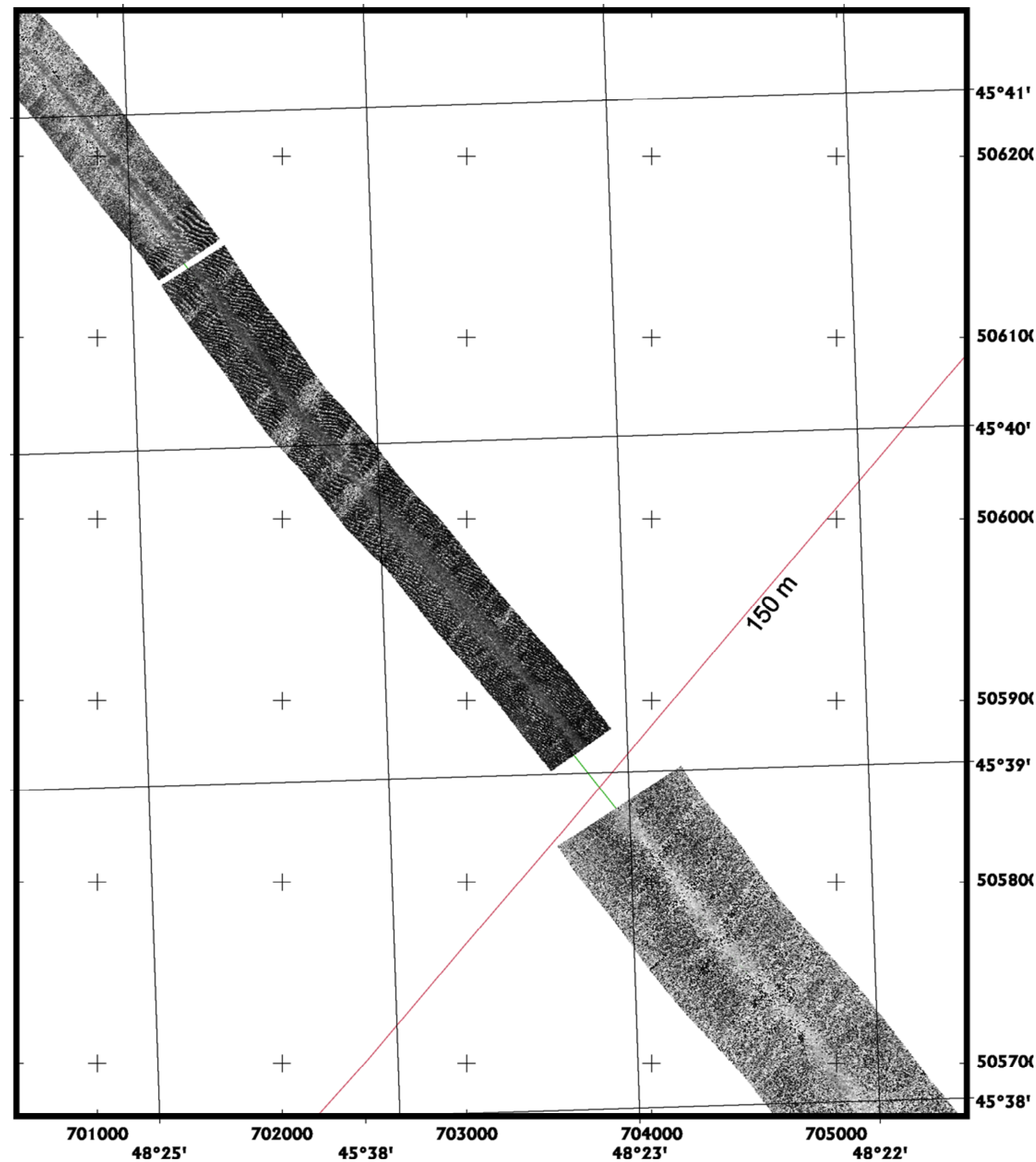

Figure 4. Sidescan image of megaripples on the upper slope (from Sonnichsen et al., 1999).

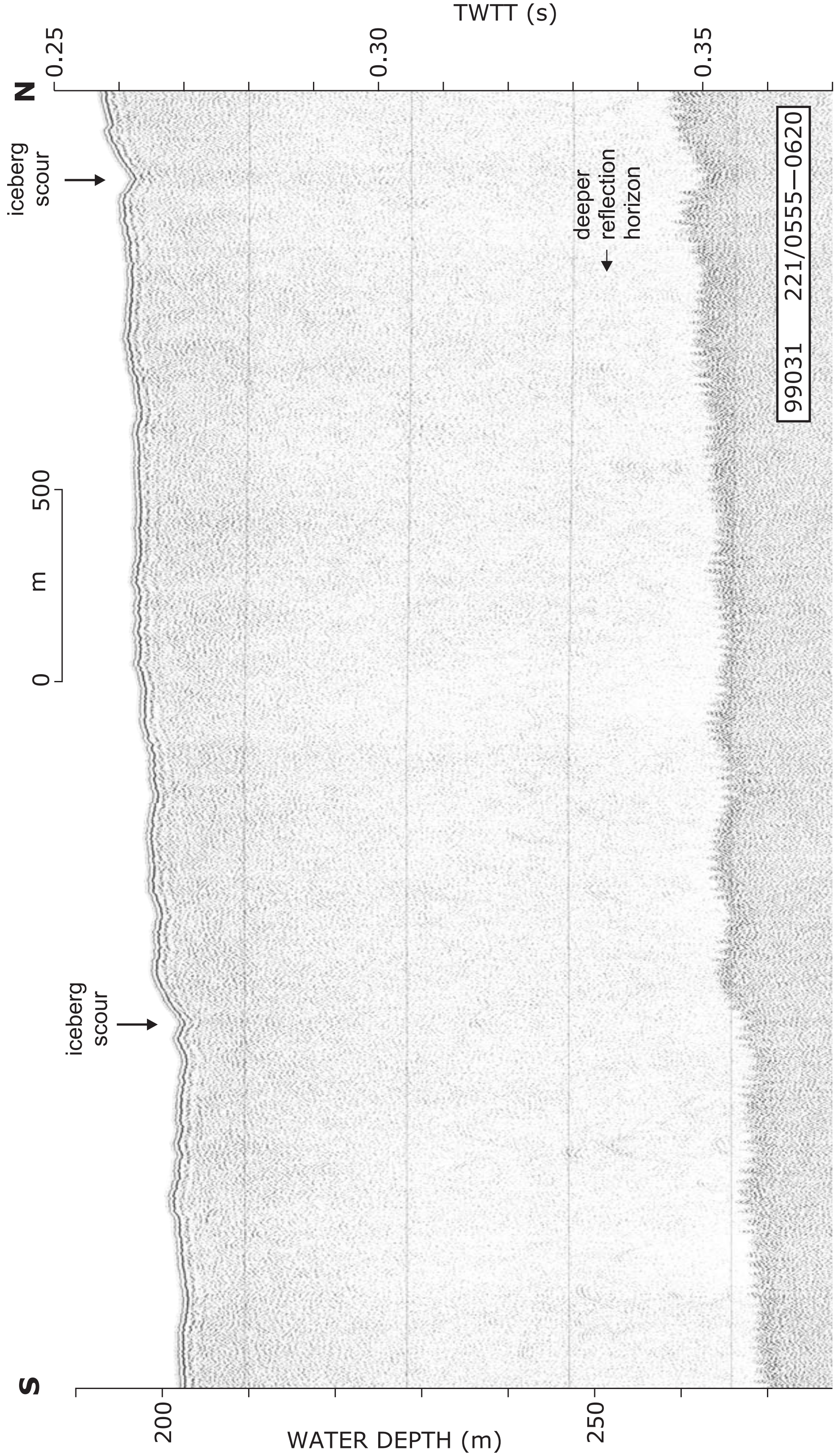

Figure 5. Type example of the till facies in the Huntec records of the upper slope. This example shows an irregular surface with a few iceberg scours, incoherent internal reflections with scattered and grouped hyperbolic reflections at about 60 ms.

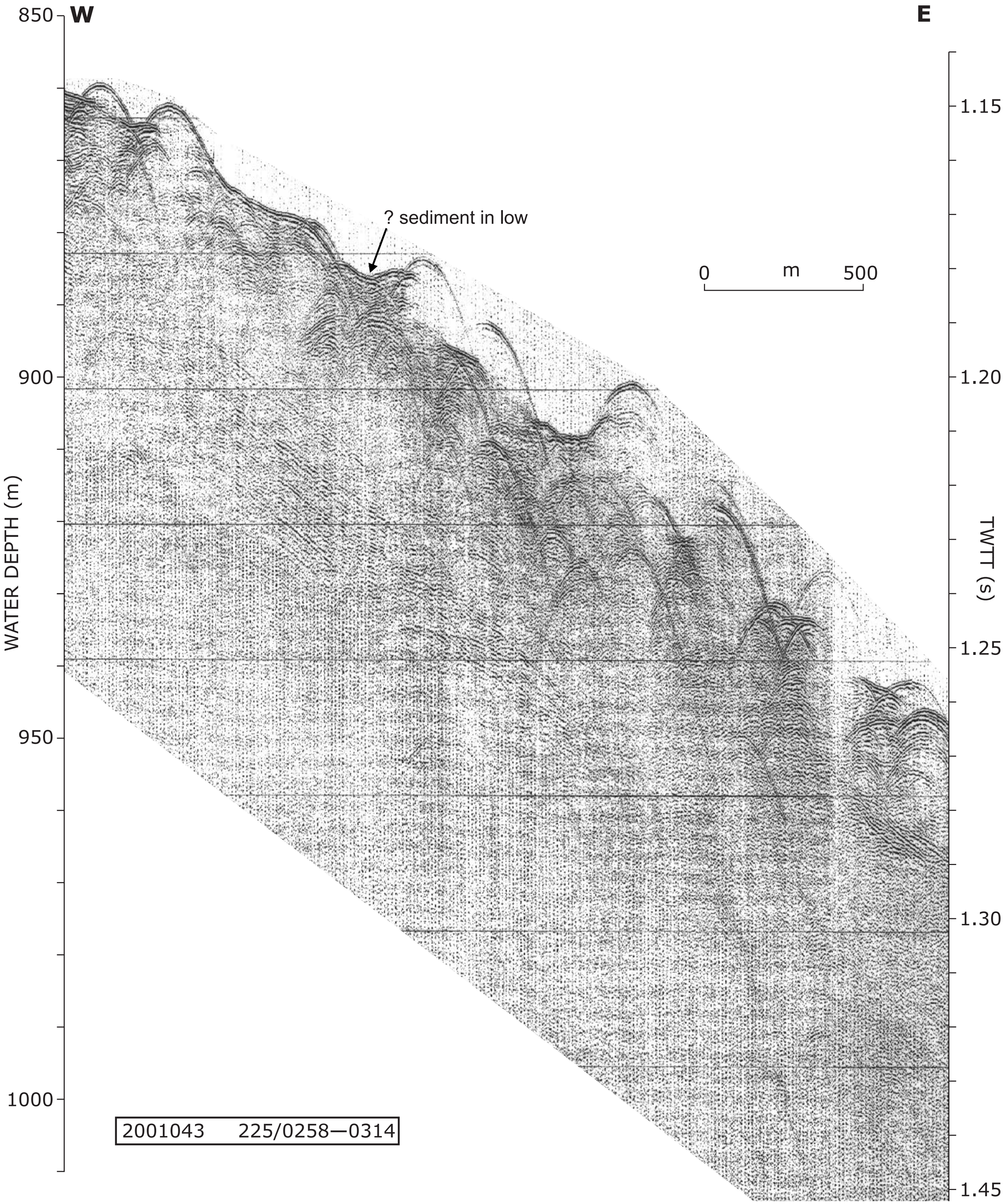

Figure 6. Type example of the hummocky middle slope facies in the Huntec records. Water acoustic energy has not been masked down to the seabed, since it is unclear where the seafloor is. Many of the hyperbolic reflections are side echoes. The underlying discontinuous reflections are cut off by the steeper overlying chaotic/incoherent reflections.

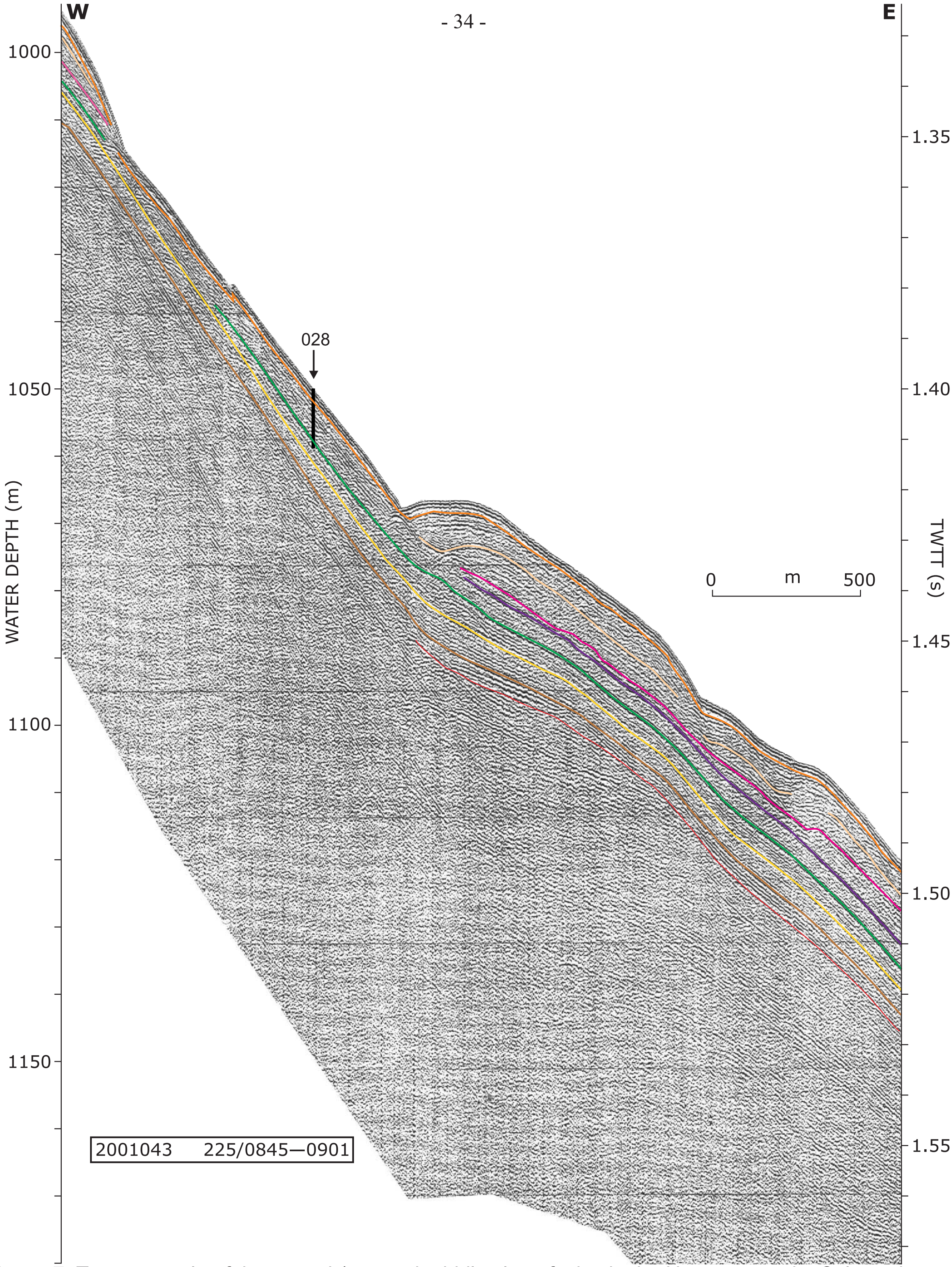

Figure 7. Type example of the smooth/scarped middle slope facies in the Huntec records. Coloured reflections are not confidently correlated with other parts of the study area.

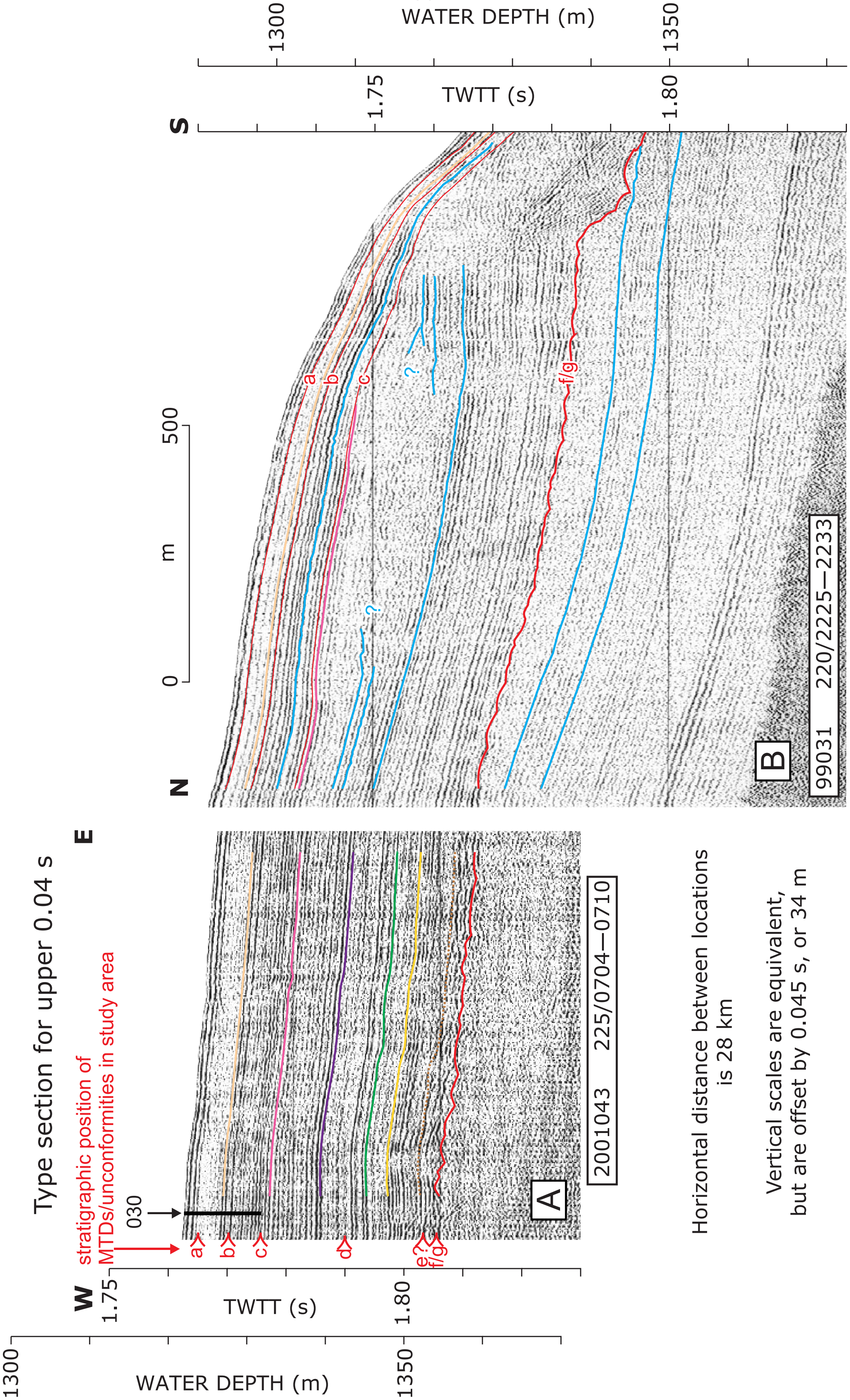

Figure 8. An example of the smooth lower slope facies in the Huntec profiles which has parallel continuous reflections. The two profiles spanning 28 km in map distance have very similar reflection profiles. (A) is the type section for the upper 0.04 s. (B) has an isolated MTD at 20 ms sub-bottom.

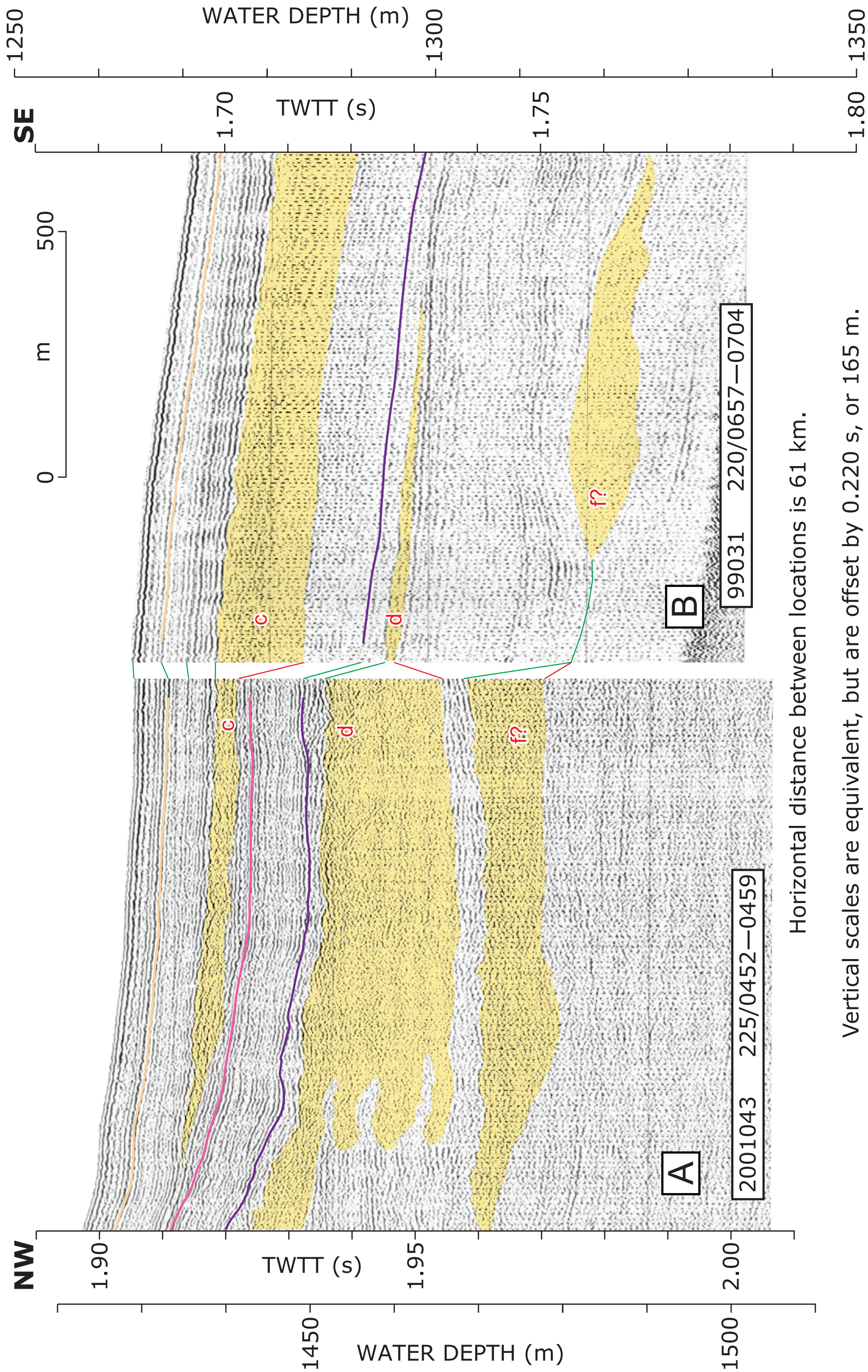

Figure 9. An example the smooth lower slope facies with stacked incoherent intervals (interpreted as MTDs) in the Huntec records. MTDs are correlated based on reflection character 61 km apart in similar water depths.

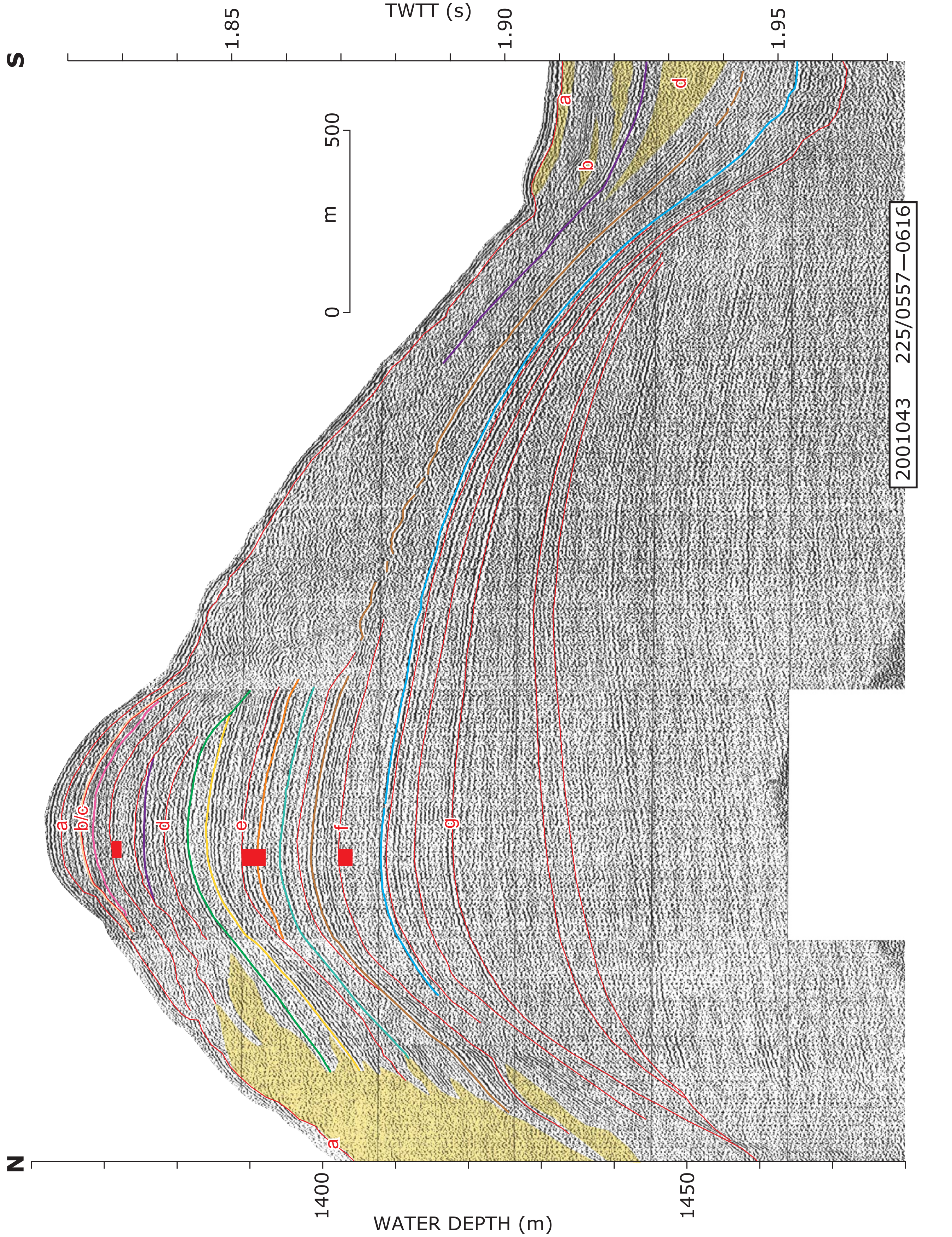

Figure 10. Huntec profile through a ridge on the lower slope, which consists of draped parallel reflection sequences with angular unconformities on the steep margins. This profile correlates well with Fig. 11. The red blocks indicate the stratigraphic intervals missing in Fig. 11. This location is also a type section for Huntec stratigraphy below 0.04 s.

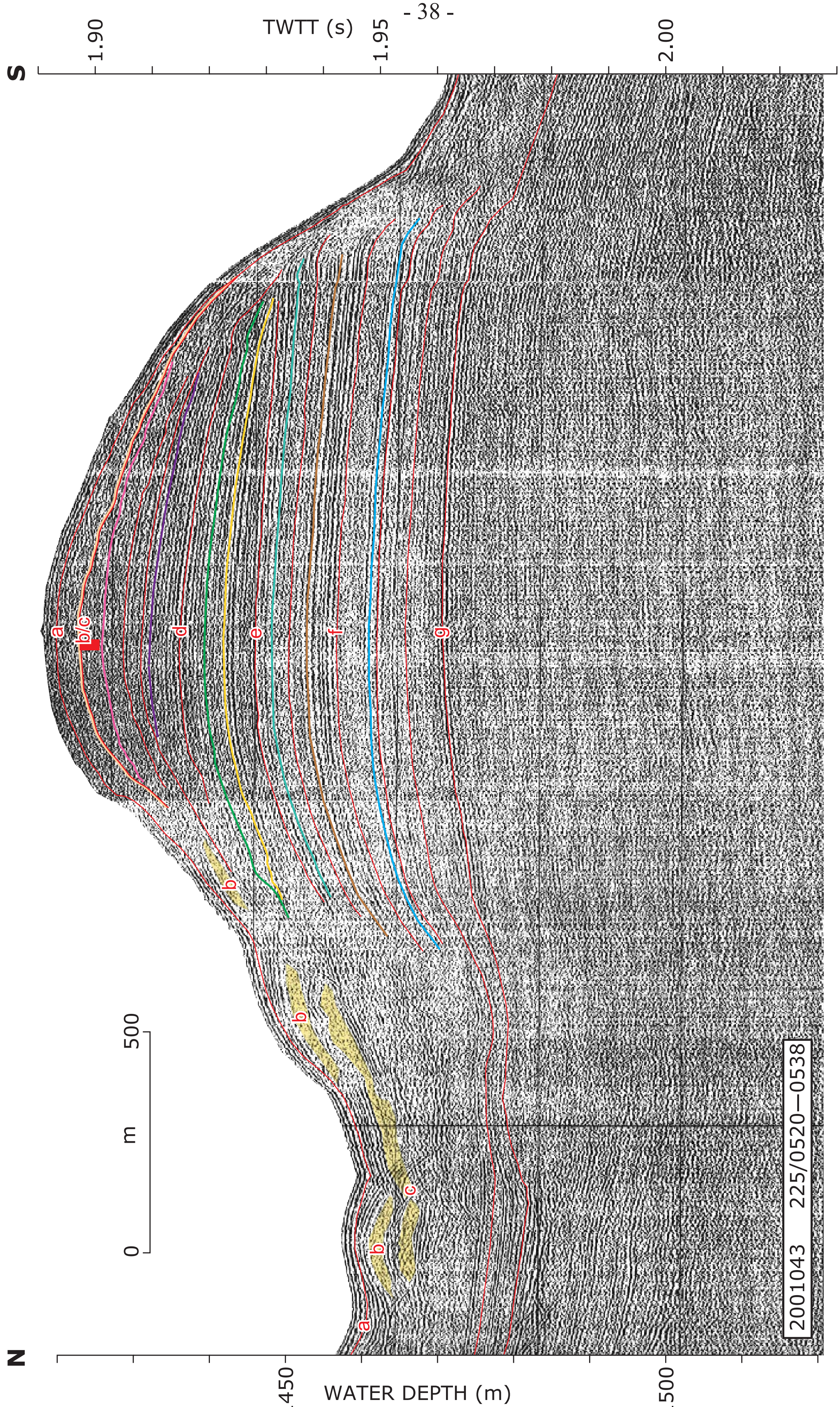

Figure 11. Huntec profile through a ridge on the lower slope. This profile is similar to Fig. 10. The red blocks indicates the stratigraphic intervals missing in Fig. 10.

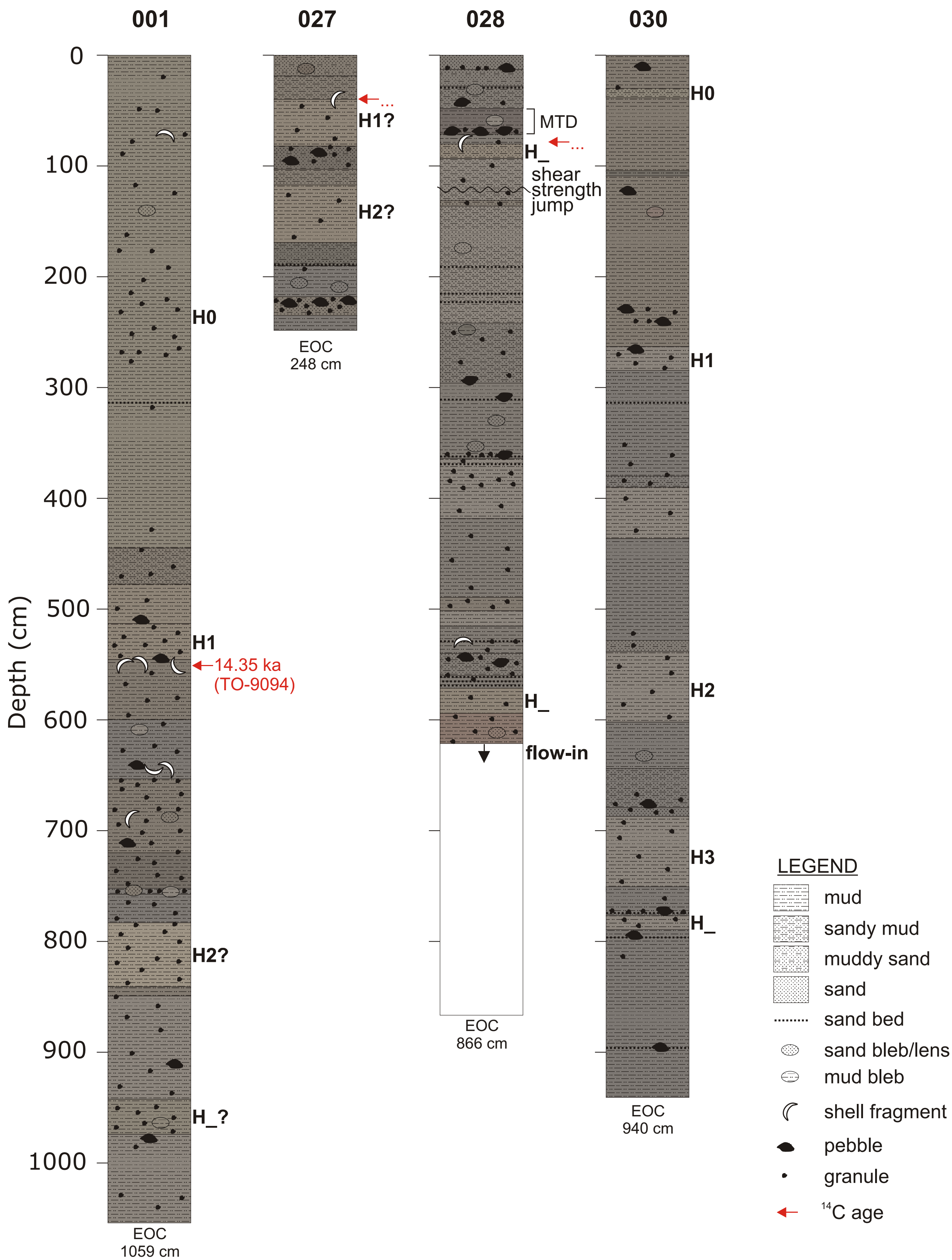

Figure 12. Summary plots of the piston cores. See appendix for more detailed figures.

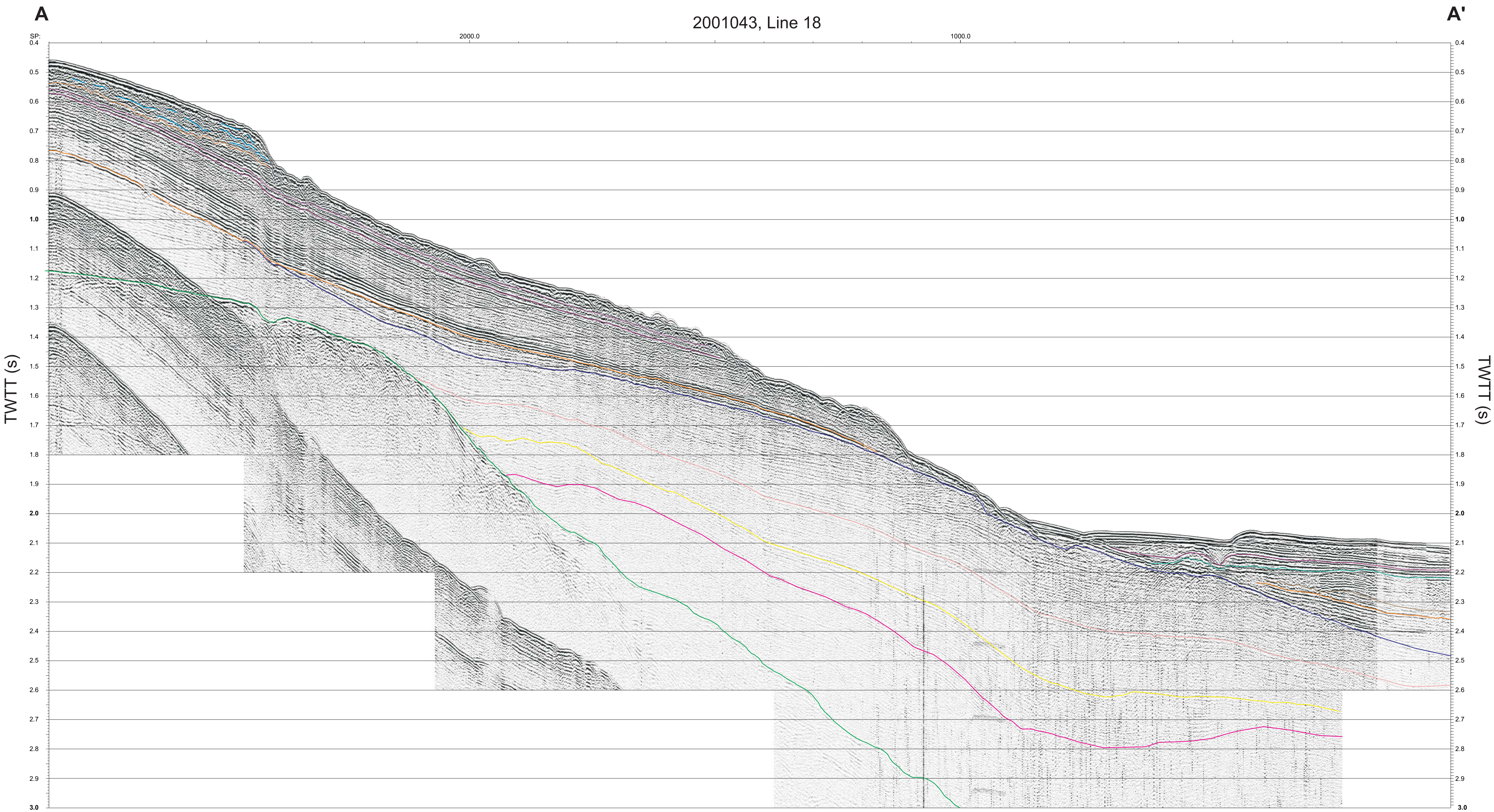

Figure 13. Single-channel airgun profile A-A´ (2001043, Line 18).

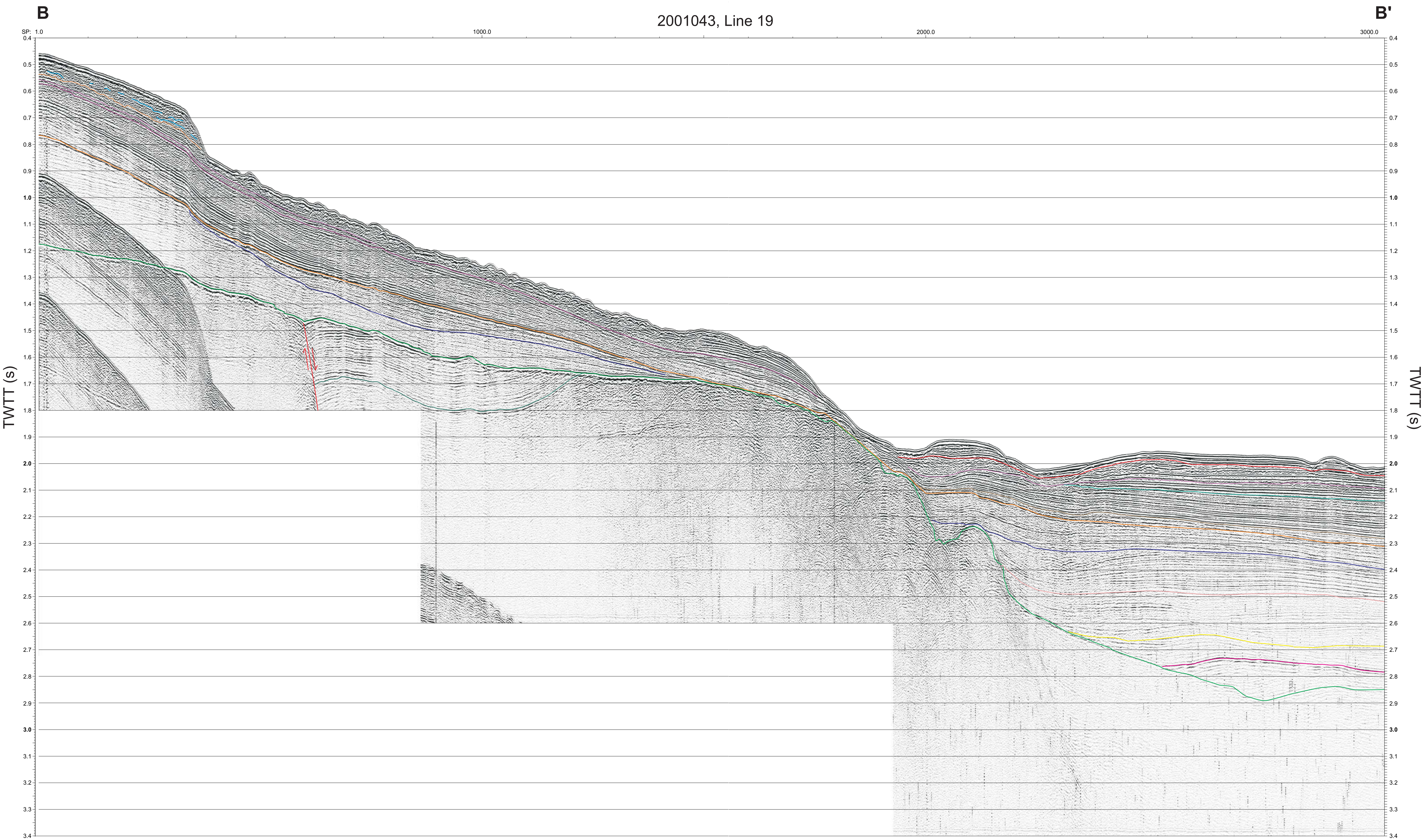

Figure 14. Single-channel airgun profile B-B´ (2001043, Line 19).

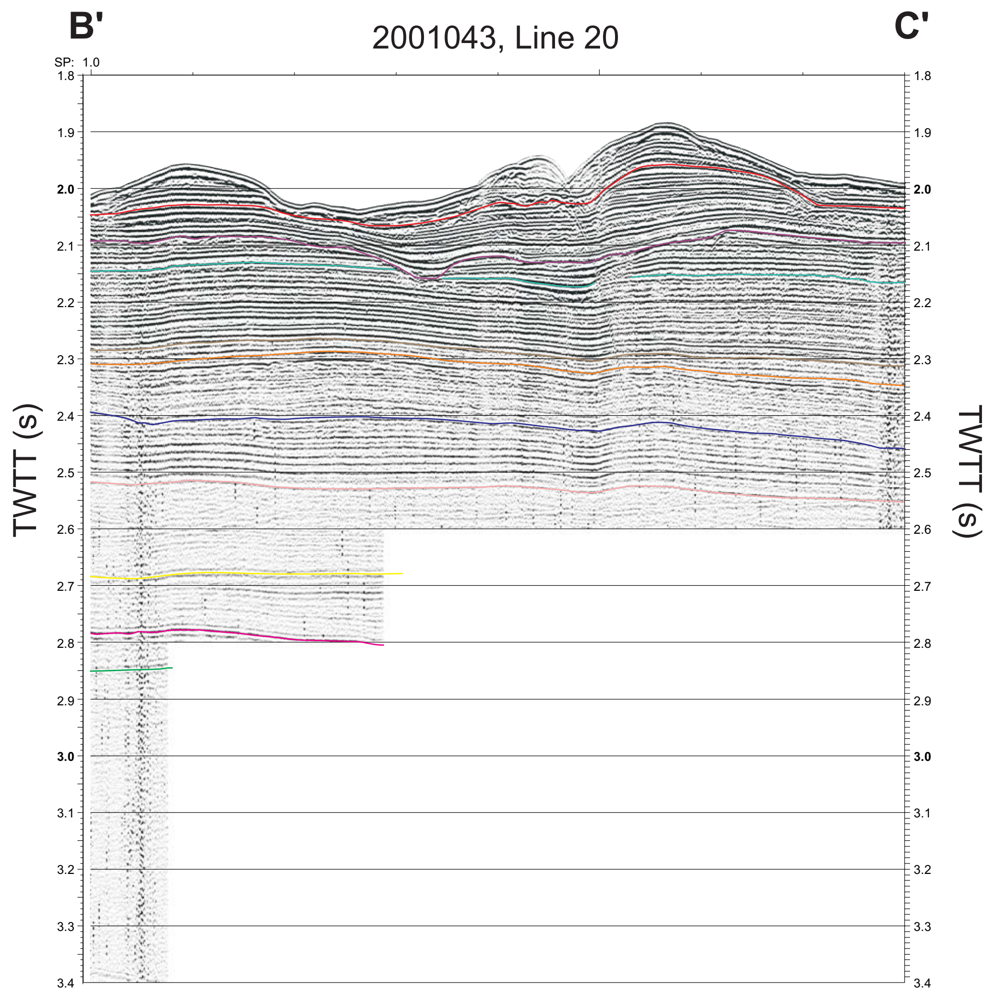

Figure 15. Single-channel airgun profile B´-C´ (2001043, Line 20).

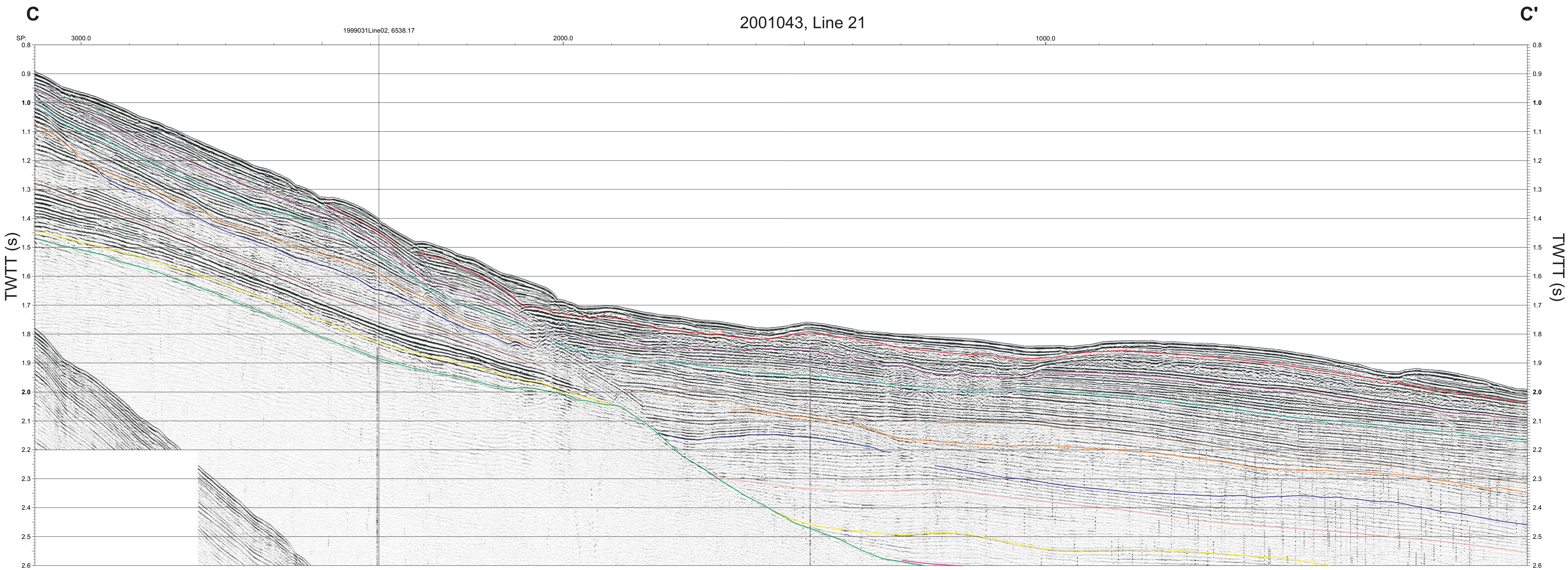

Figure 16. Single-channel airgun profile C-C´ (2001043, Line 21).

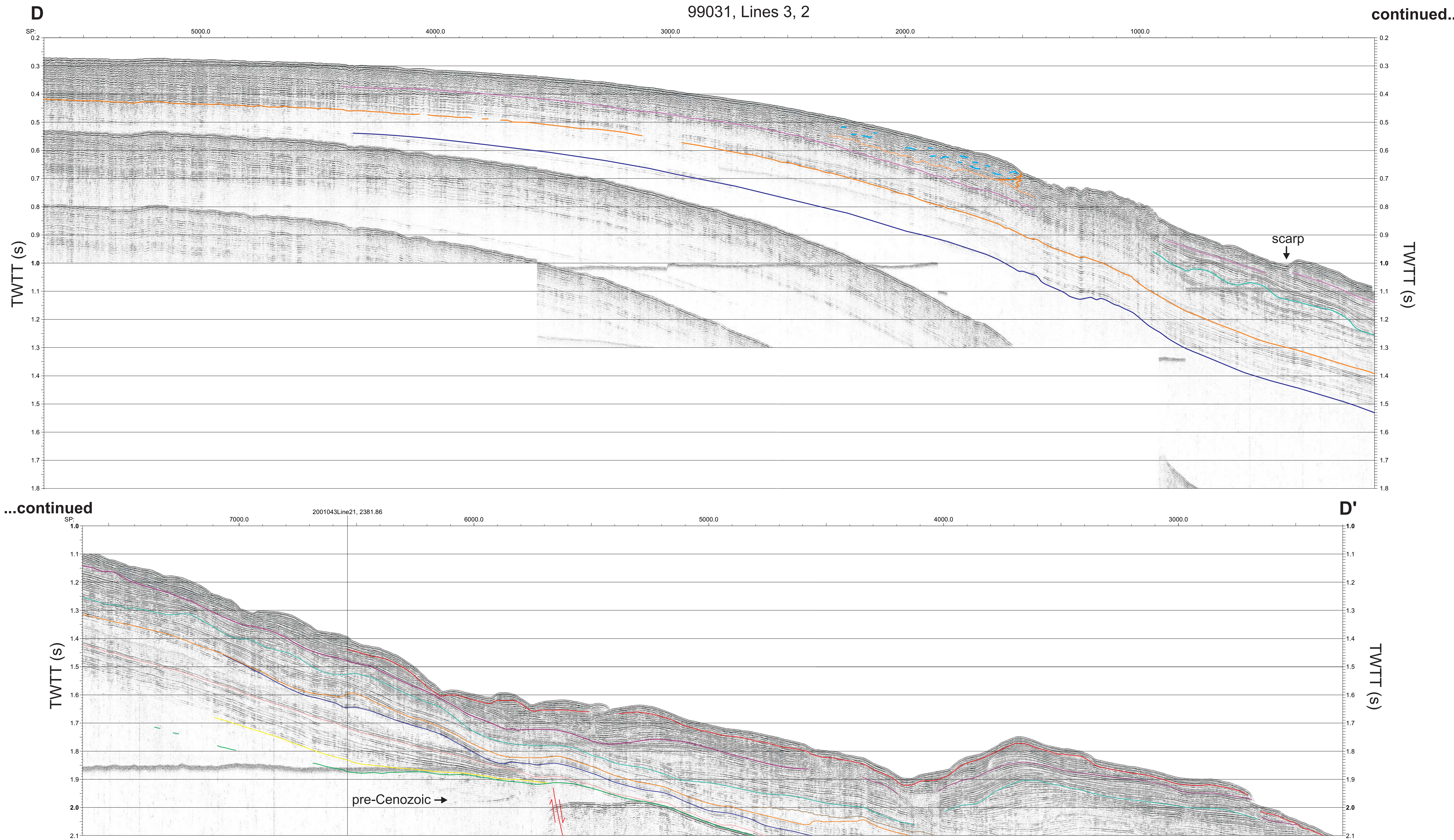

Figure 17. Single-channel airgun profile D-D´ (99031, Lines 2, 3).

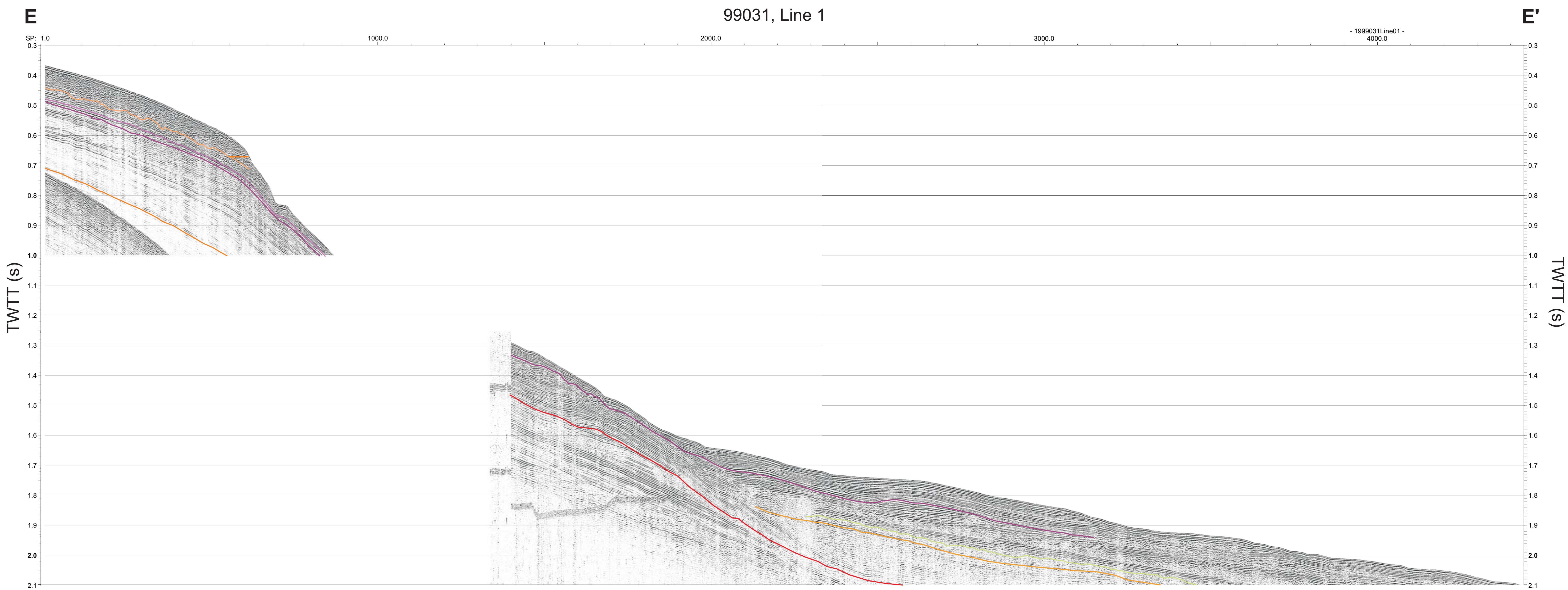

Figure 18. Single-channel airgun profile E-E´ (99031, Line 1).

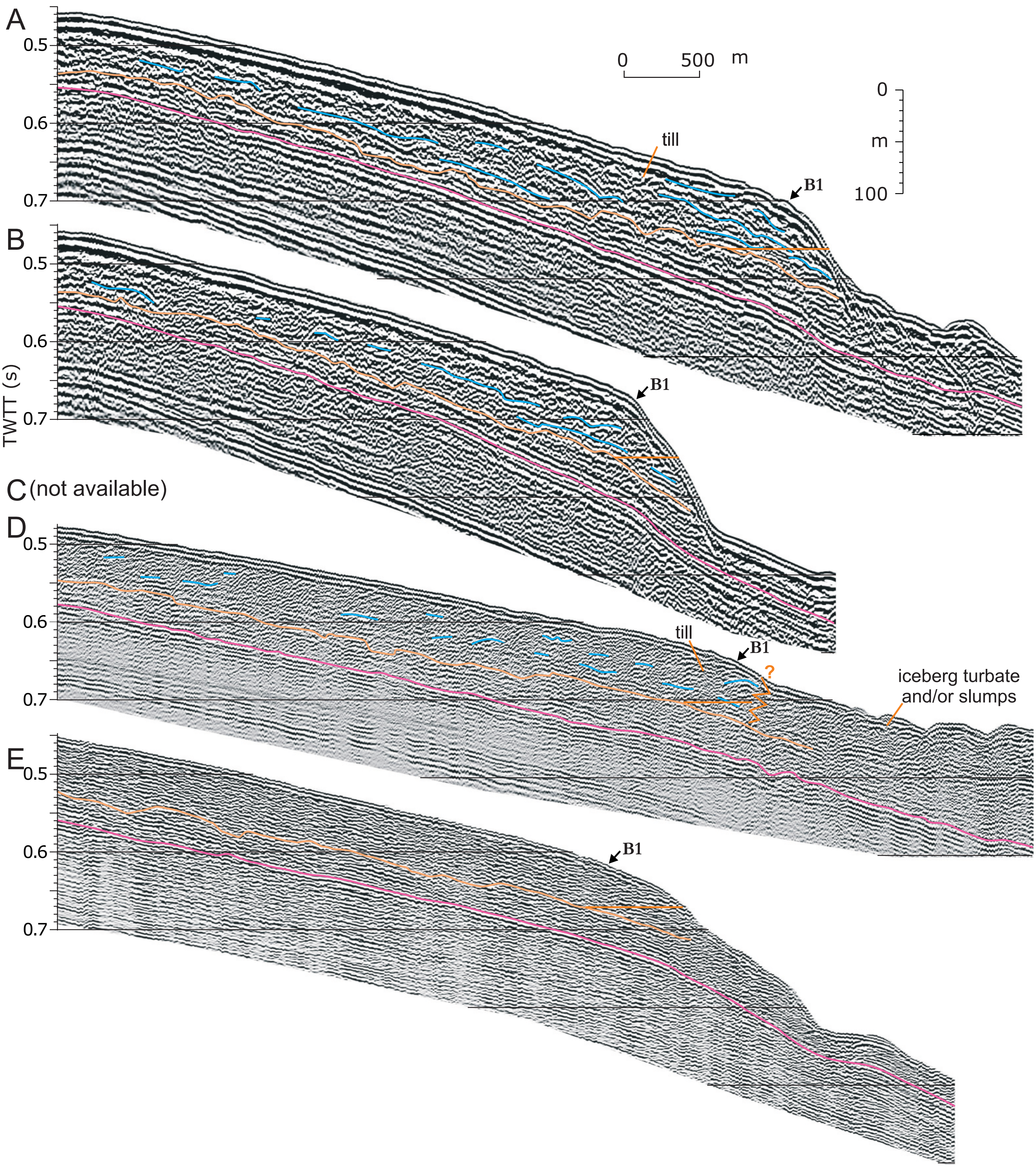

Figure 19. High-resolution airgun profiles through the upper slope. Locations of (A), (B), (D) and (E) are in Fig. 2.

Appendix A

Detailed logs of piston cores and trigger weight cores

LEGEND

- mud
- sandy mud
- muddy sand
- sand
- sand bed
- sand bleb/lens
- mud bleb
- shell fragment
- pebble
- granule
- ^{14}C age

Hudson 1999-031 TWC 001

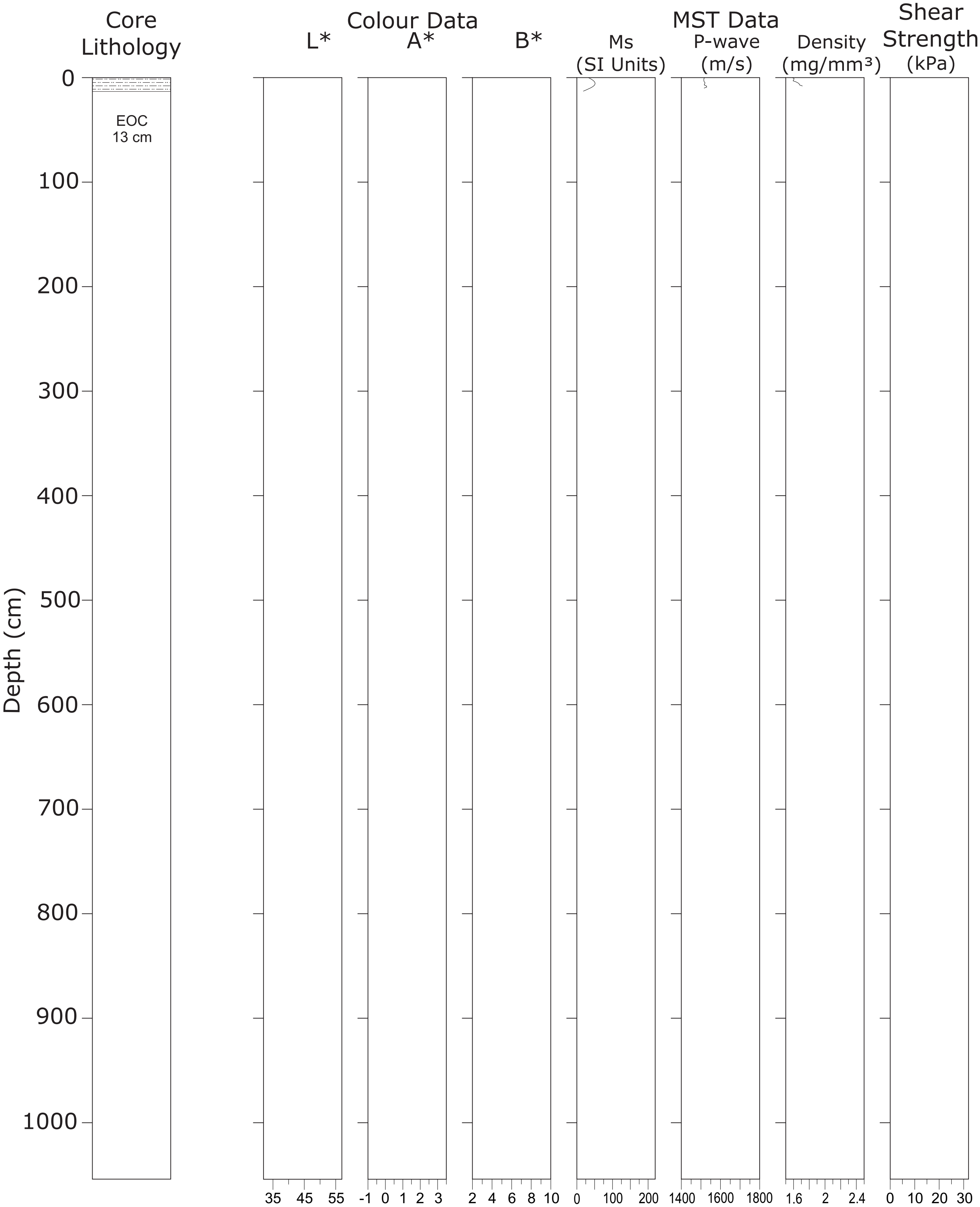

Hudson 1999-031 Piston Core 001

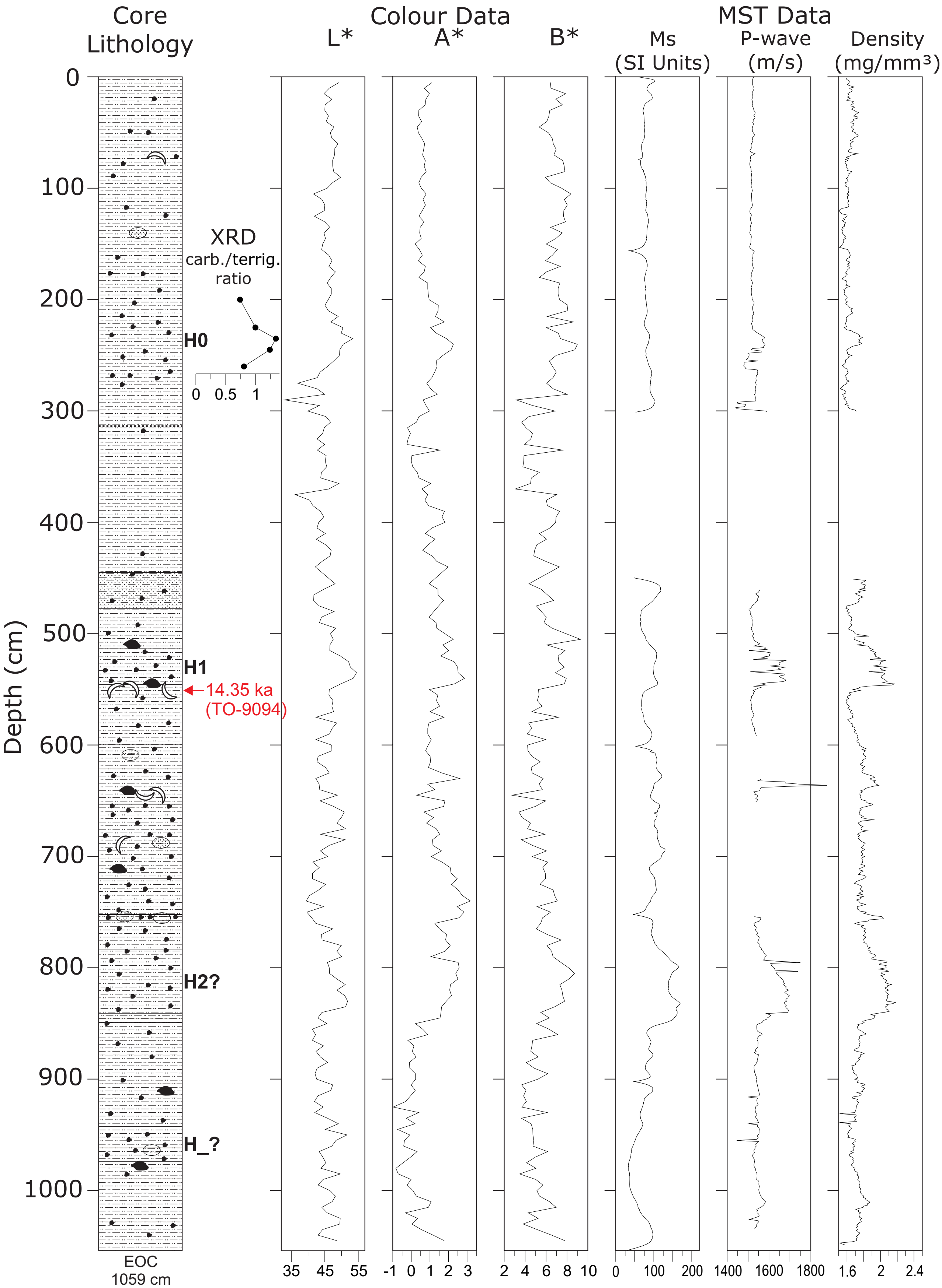

Hudson 2001-043 Piston Core 027

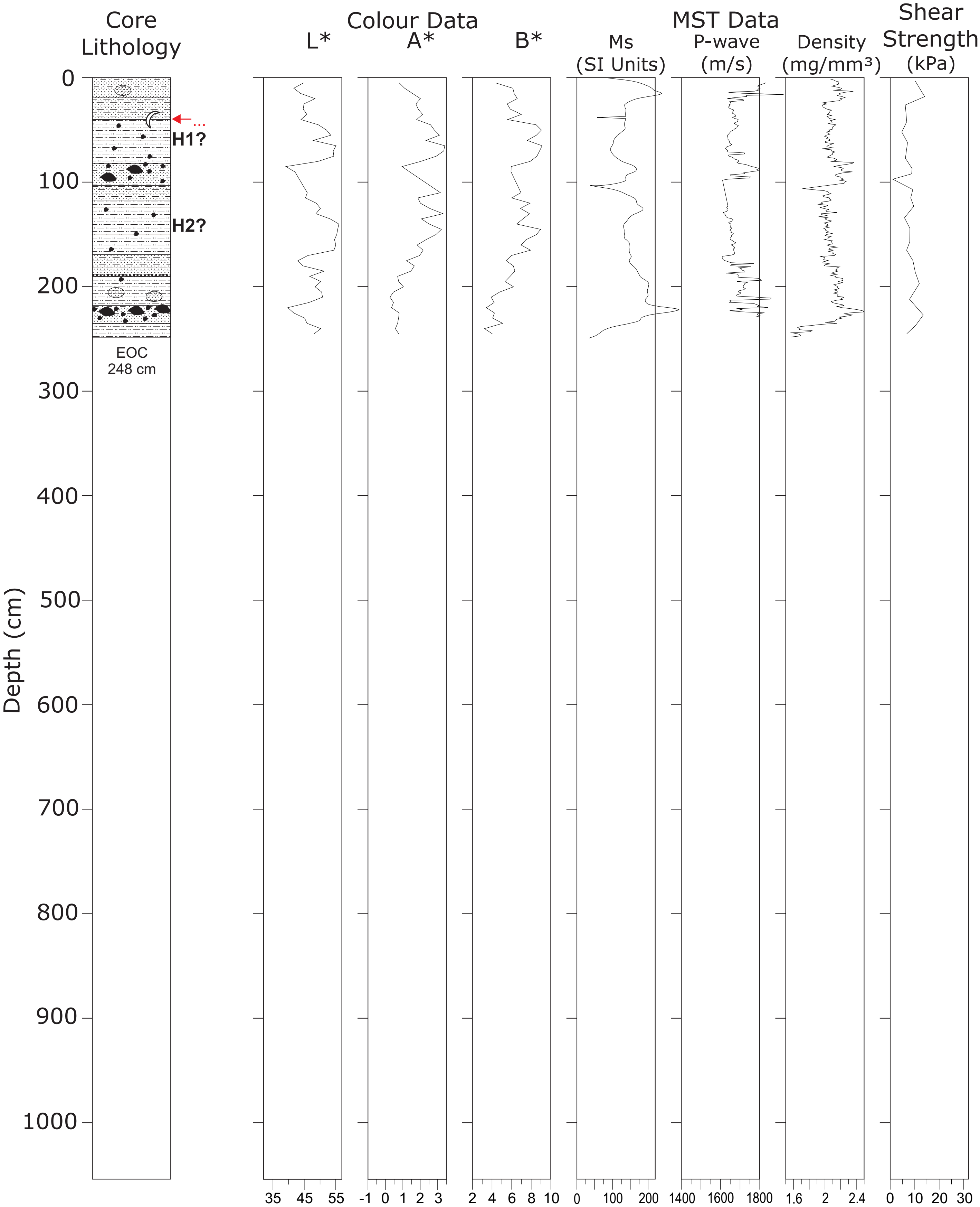

Hudson 2001-043 TWC 028

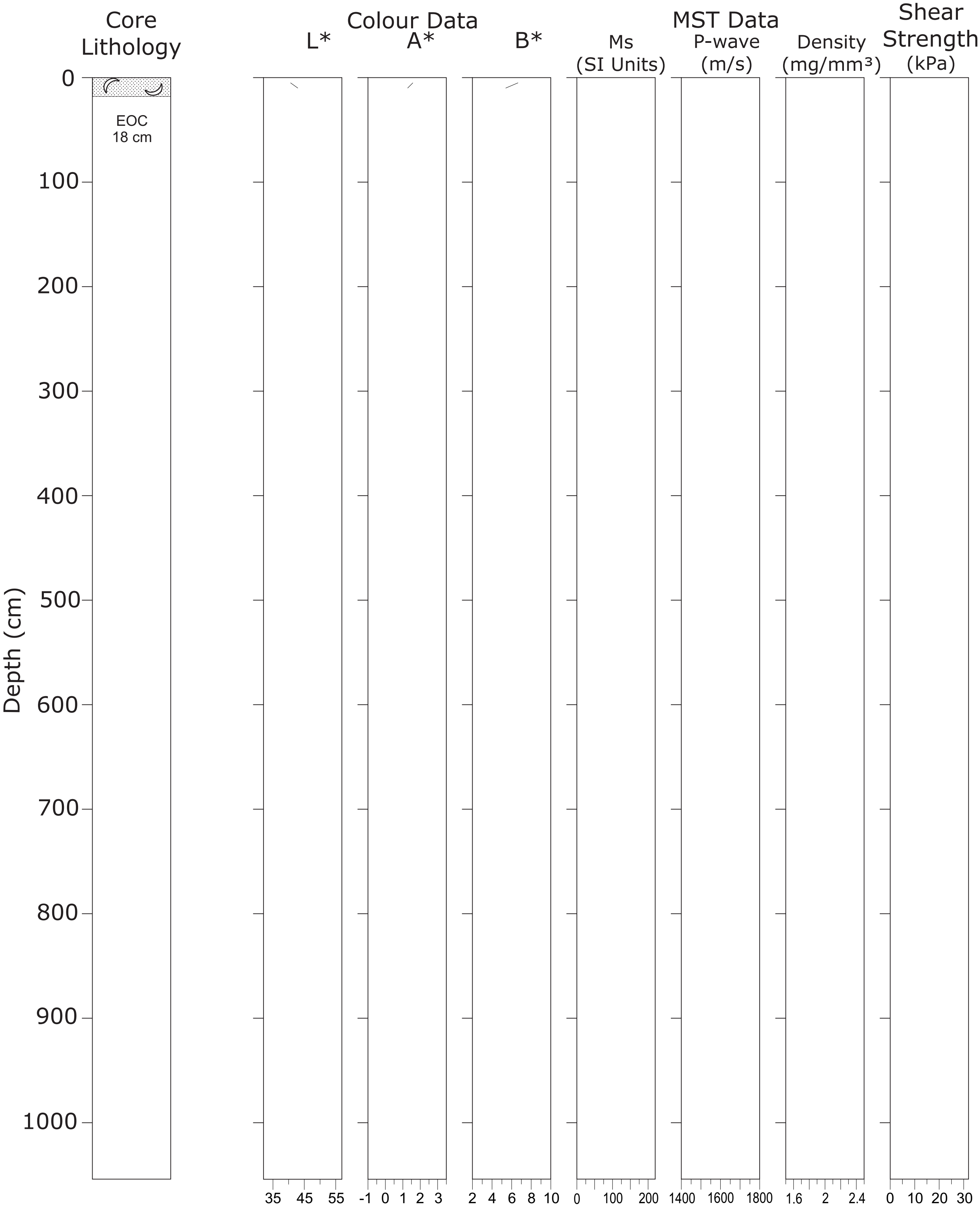

Hudson 2001-043 Piston Core 028

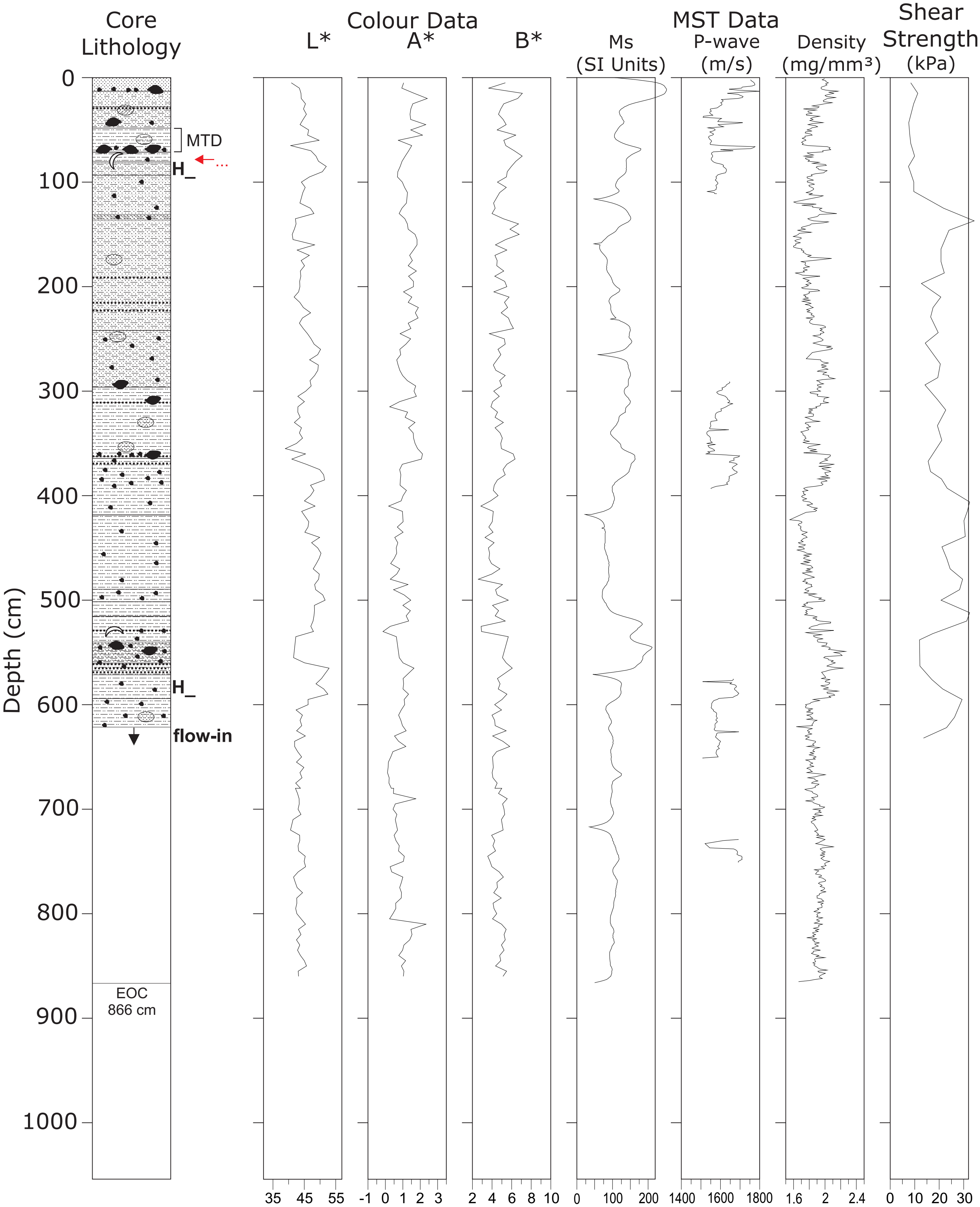

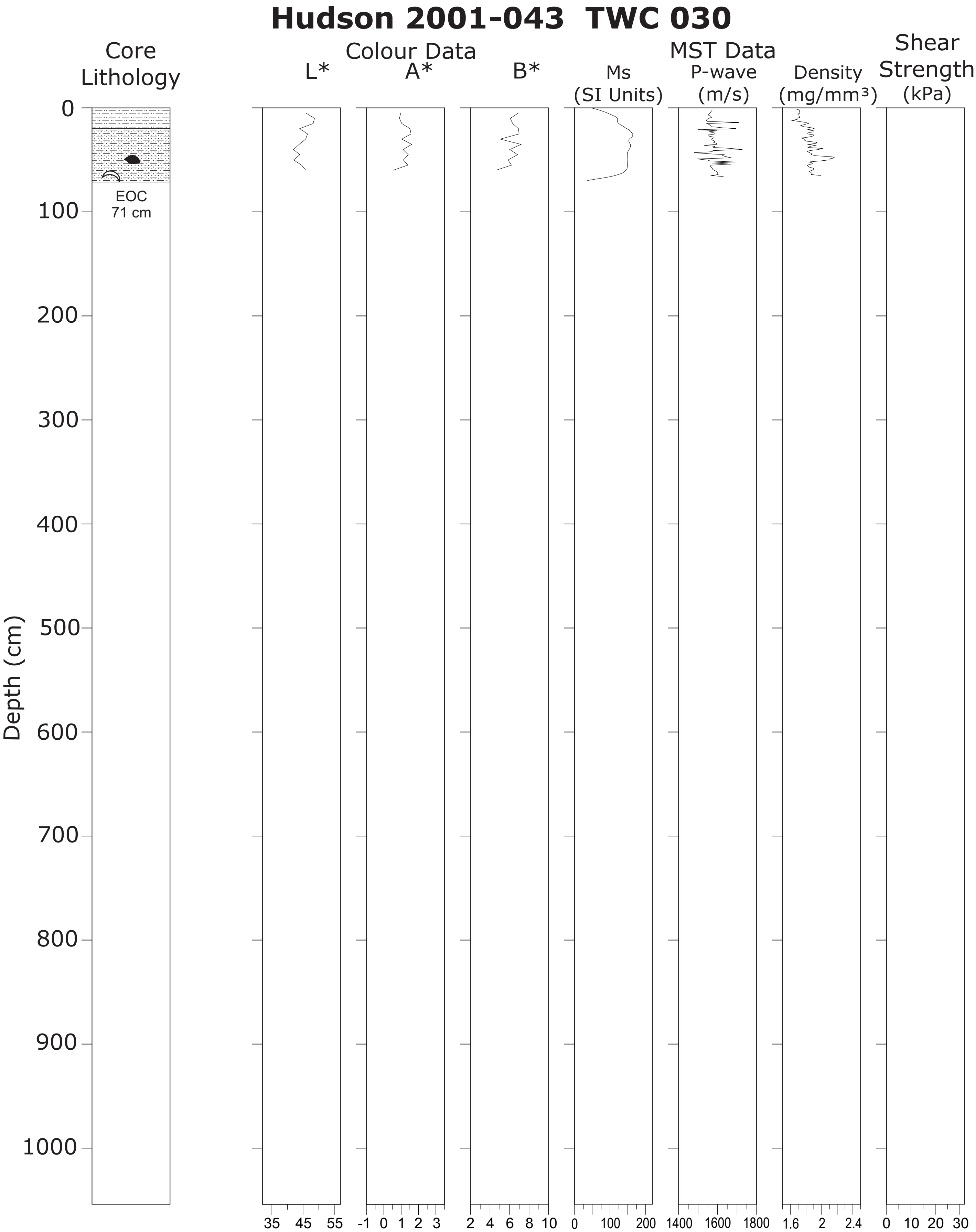
Hudson 2001-043 TWC 030
Core Lithology
Colour Data
L*
A*
B*
MST Data
Ms (SI Units)
P-wave (m/s)
Density (mg/mm³)
Shear Strength (kPa)
EOC 71 cm
Depth (cm)
0
100
200
300
400
500
600
700
800
900
1000
35 45 55
-1 0 1 2 3
2 4 6 8 10
0 100 200
1400 1600 1800
1.6 2 2.4
0 10 20 30

Hudson 2001-043 Piston Core 030

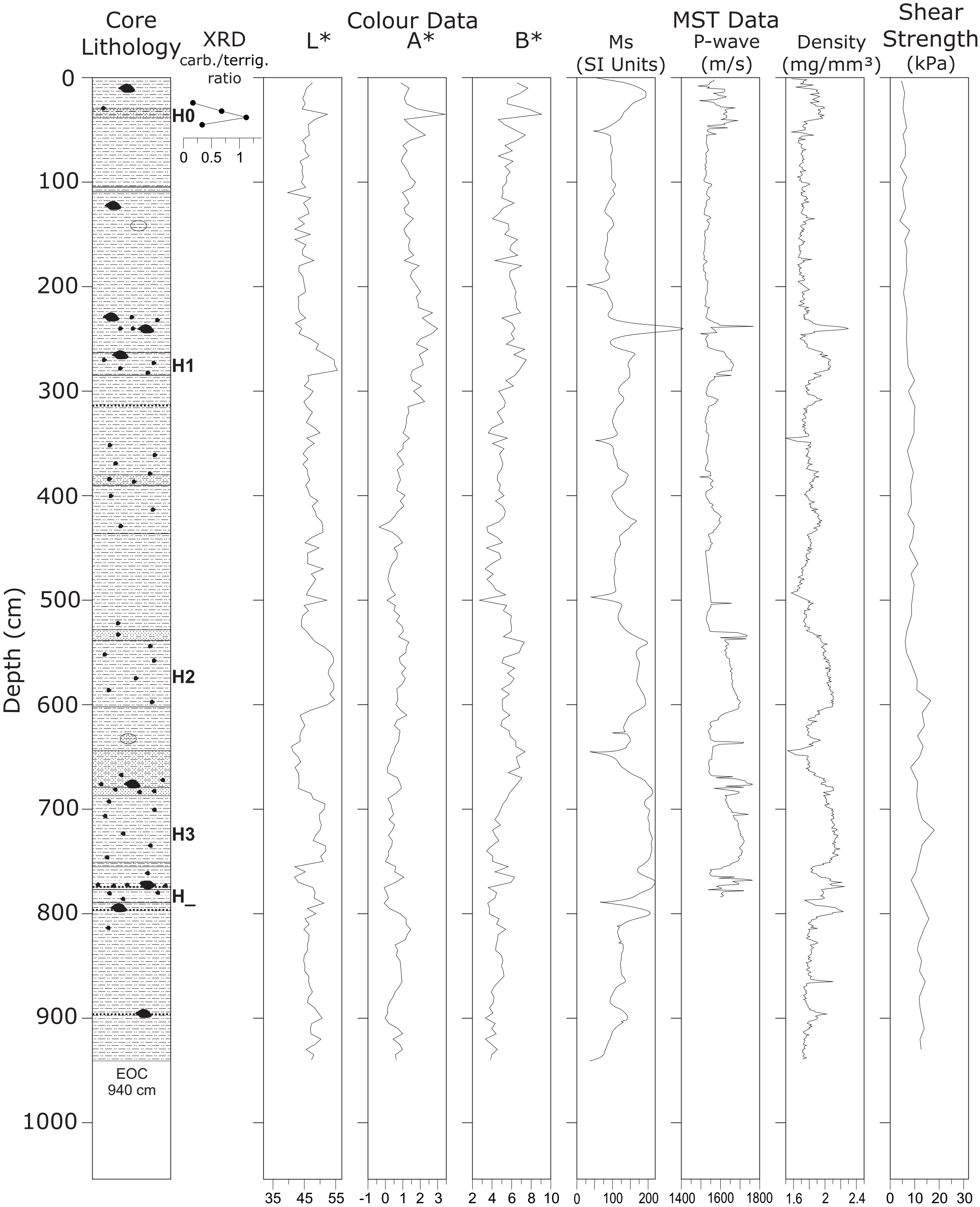

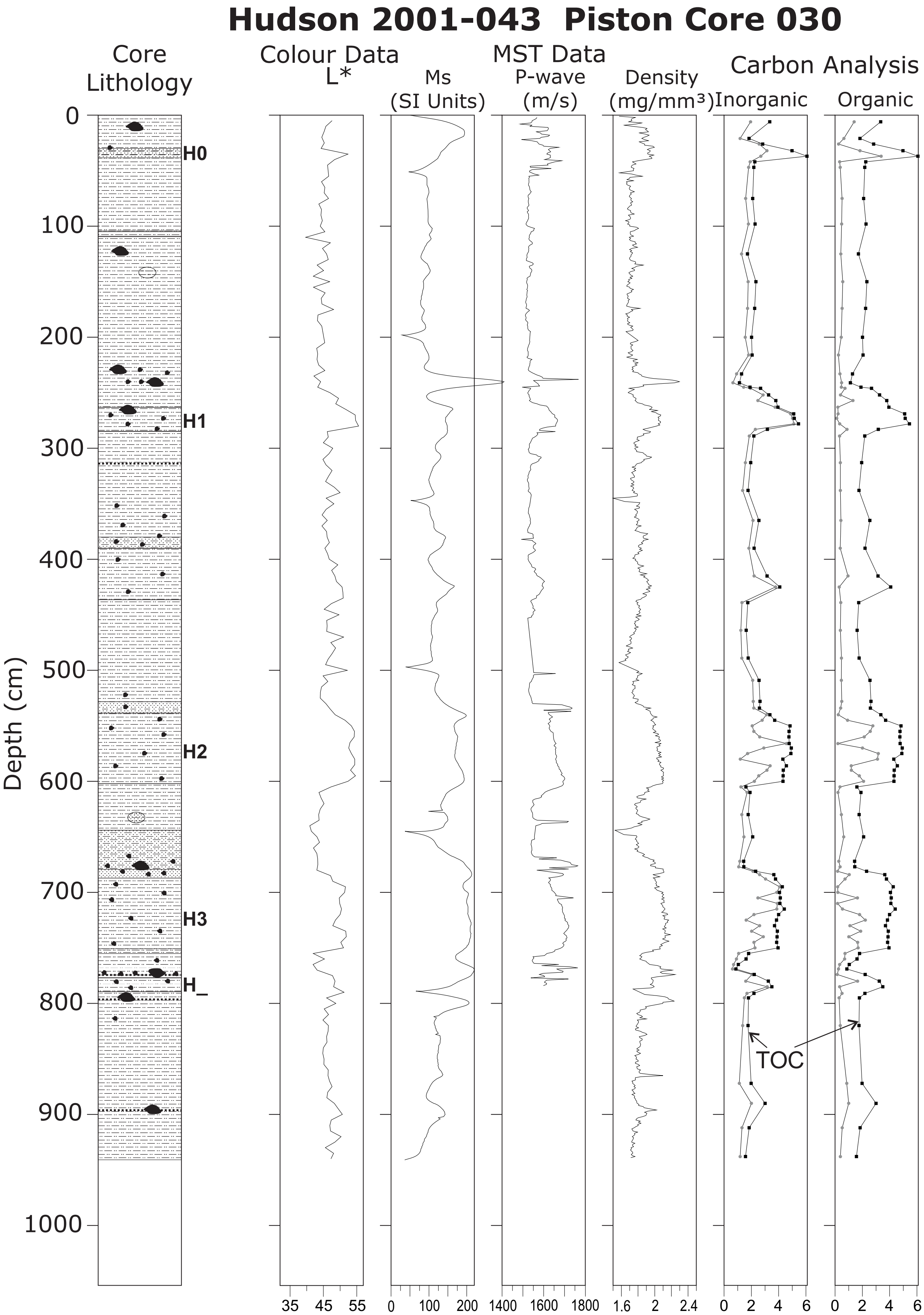
Hudson 2001-043 Piston Core 030
Core Lithology
Colour Data
L*
MST Data
Ms
(SI Units)
P-wave
(m/s)
Density
(mg/mm³)
Carbon Analysis
Inorganic
Organic
Depth (cm)
0
100
200
300
400
500
600
700
800
900
1000
H0
H1
H2
H3
H_
TOC
35
45
55
0
100
200
1400
1600
1800
1.6
2
2.4
0
2
4
6
0
2
4
6

Hudson 2001-043 Piston Core 030

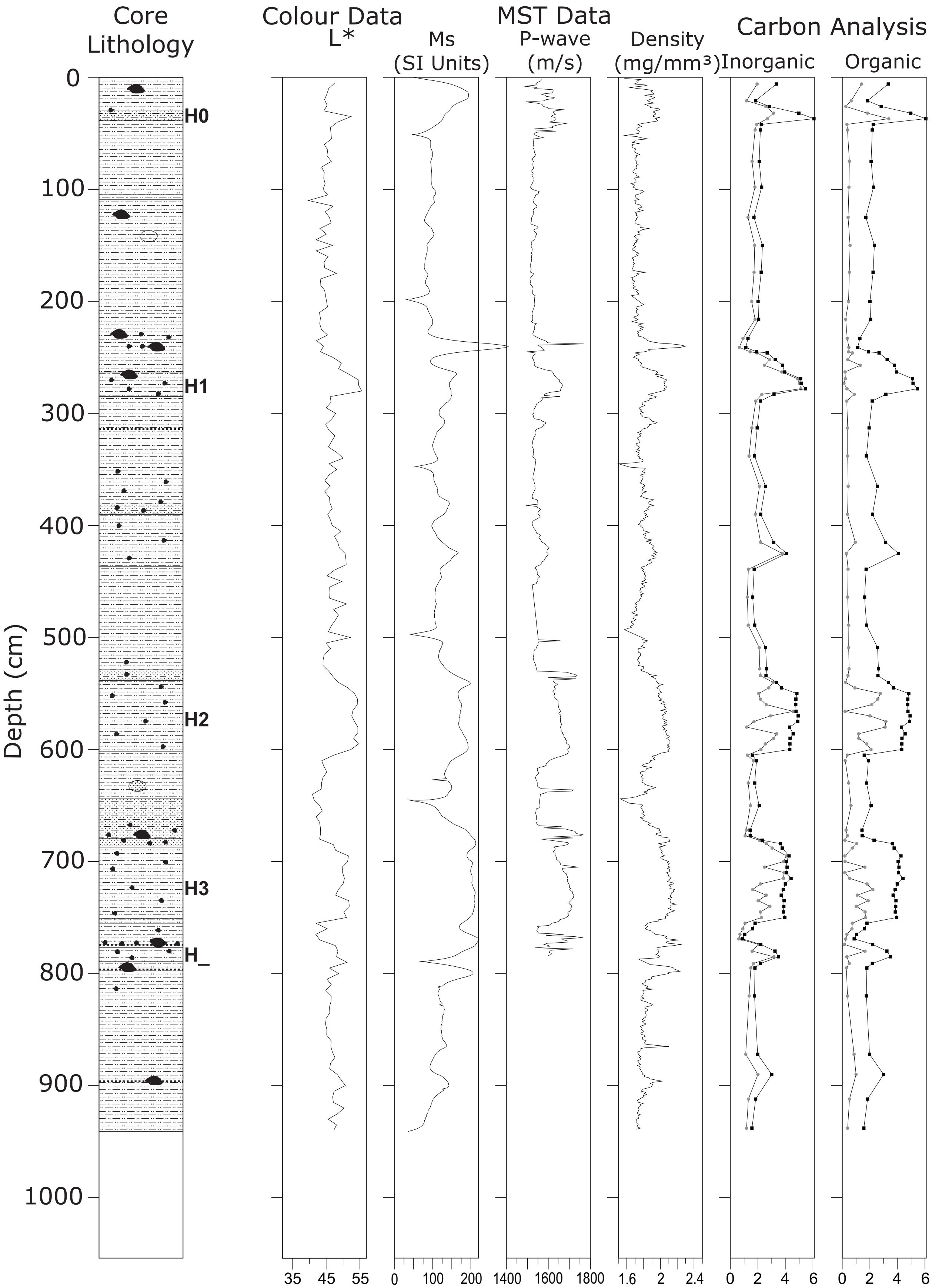

Appendix B

Uninterpreted single-channel airgun profiles

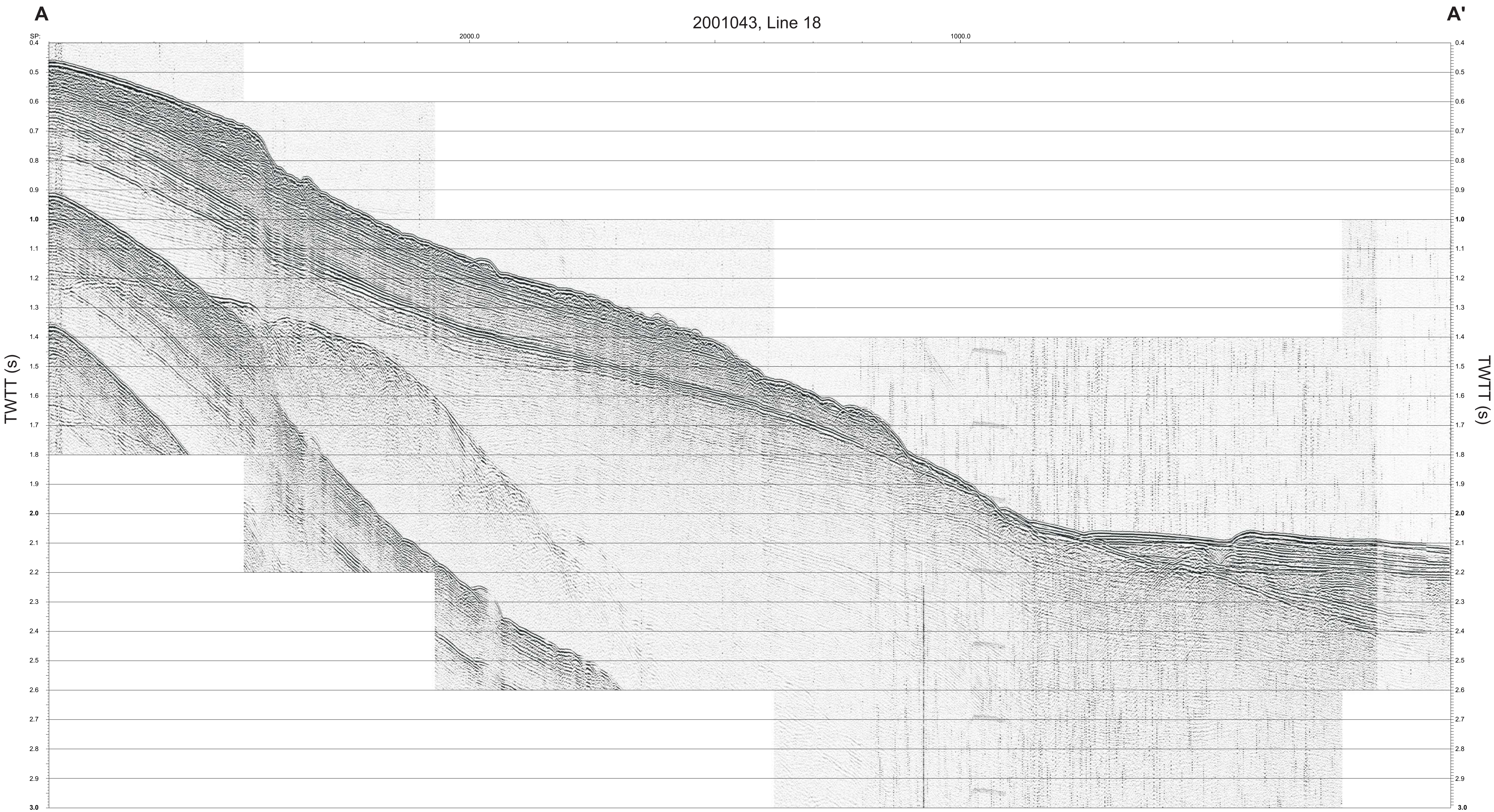
A
A'
2001043, Line 18
SP:
2000.0
1000.0
TWTT (s)
TWTT (s)
0.4
0.5
0.6
0.7
0.8
0.9
1.0
1.1
1.2
1.3
1.4
1.5
1.6
1.7
1.8
1.9
2.0
2.1
2.2
2.3
2.4
2.5
2.6
2.7
2.8
2.9
3.0

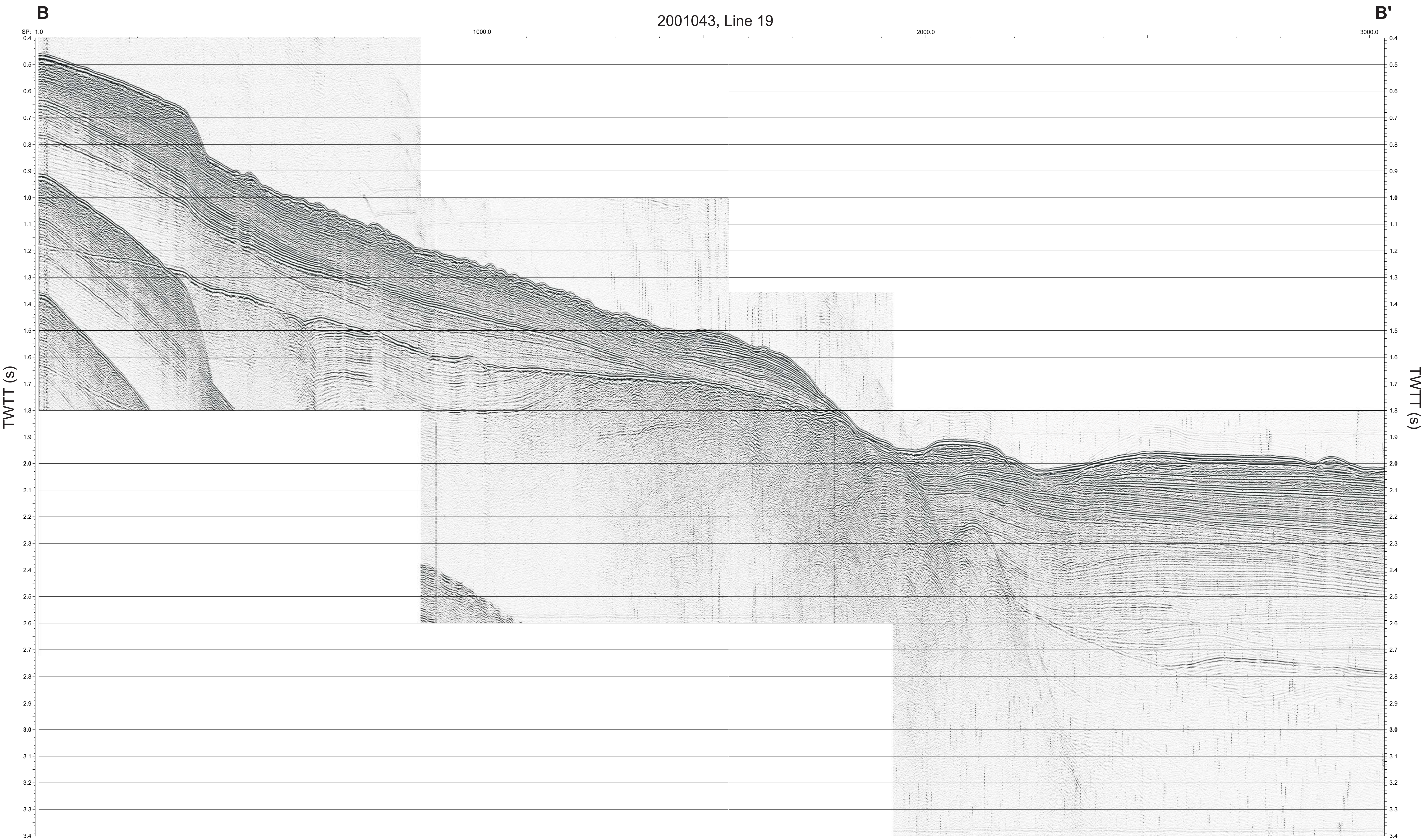
B
2001043, Line 19
B'
SP: 1.0
1000.0
2000.0
3000.0
TWTT (s)
TWTT (s)
0.4
0.5
0.6
0.7
0.8
0.9
1.0
1.1
1.2
1.3
1.4
1.5
1.6
1.7
1.8
1.9
2.0
2.1
2.2
2.3
2.4
2.5
2.6
2.7
2.8
2.9
3.0
3.1
3.2
3.3
3.4

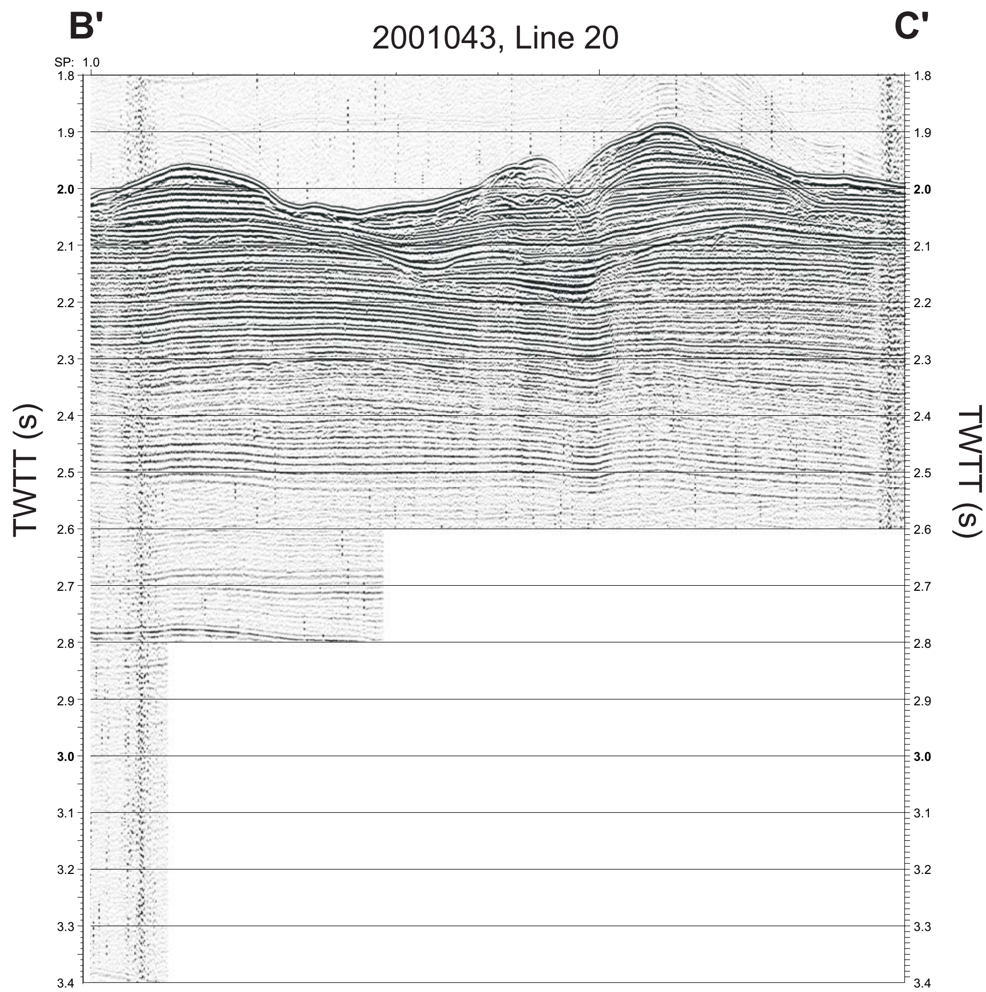

B'
2001043, Line 20
C'
SP: 1.0
TWTT (s)
1.8
1.9
2.0
2.1
2.2
2.3
2.4
2.5
2.6
2.7
2.8
2.9
3.0
3.1
3.2
3.3
3.4

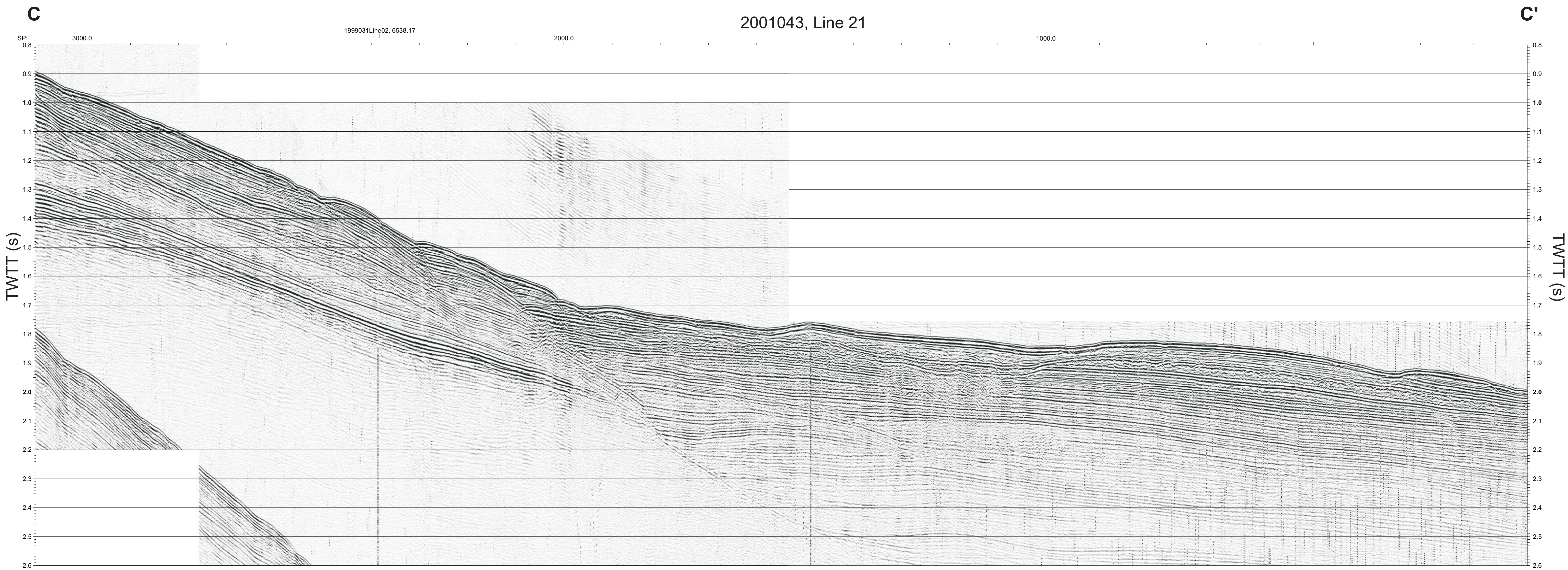
C
C'
2001043, Line 21
SP:
3000.0
1999031Line02, 6538.17
2000.0
1000.0
TWTT (s)
TWTT (s)
0.8
0.9
1.0
1.1
1.2
1.3
1.4
1.5
1.6
1.7
1.8
1.9
2.0
2.1
2.2
2.3
2.4
2.5
2.6

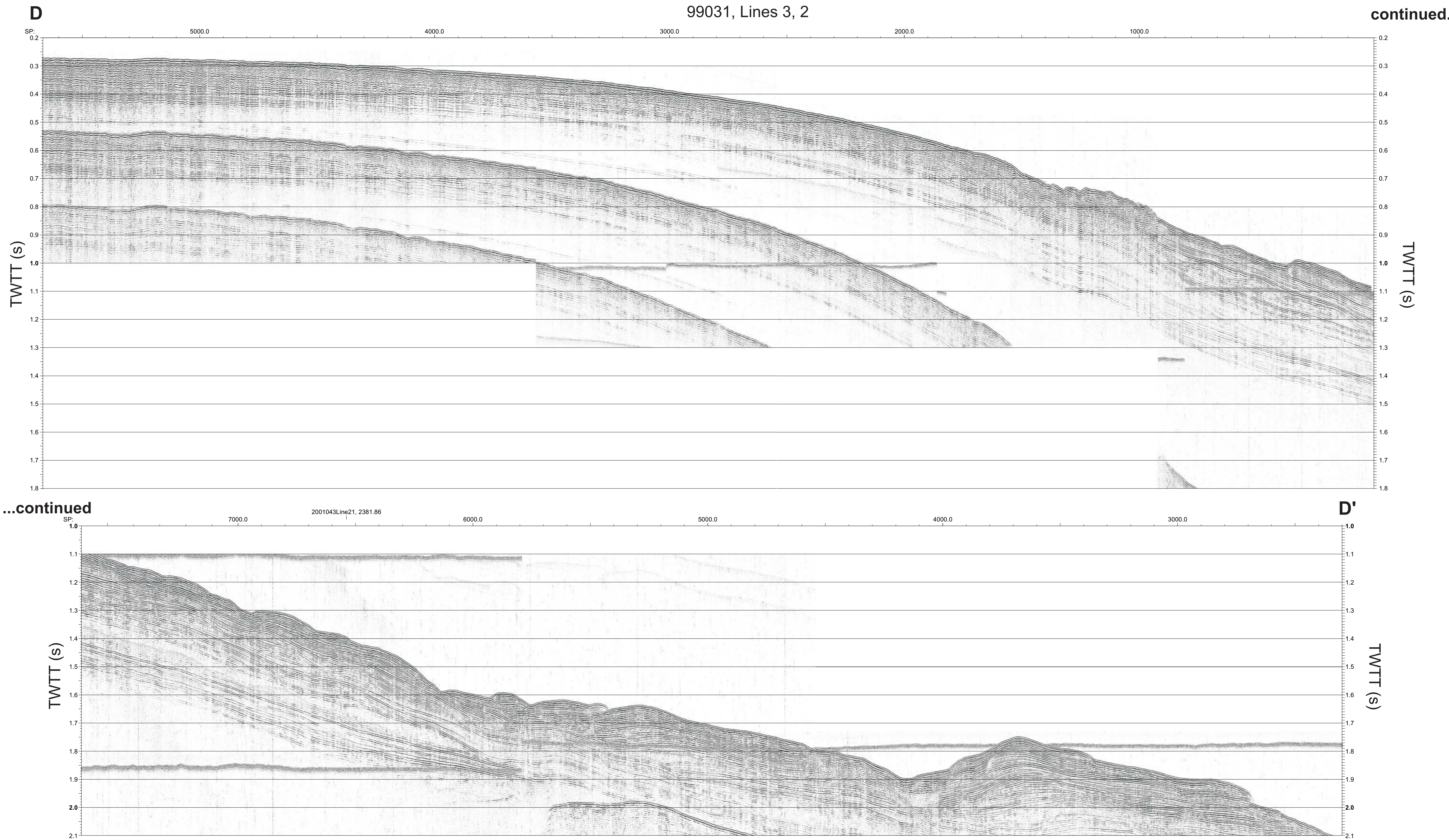
D
99031, Lines 3, 2
continued...
SP:
5000.0
4000.0
3000.0
2000.0
1000.0
TWTT (s)
TWTT (s)
...continued
D'
2001043Line21, 2381.86
7000.0
6000.0
5000.0
4000.0
3000.0
TWTT (s)
TWTT (s)

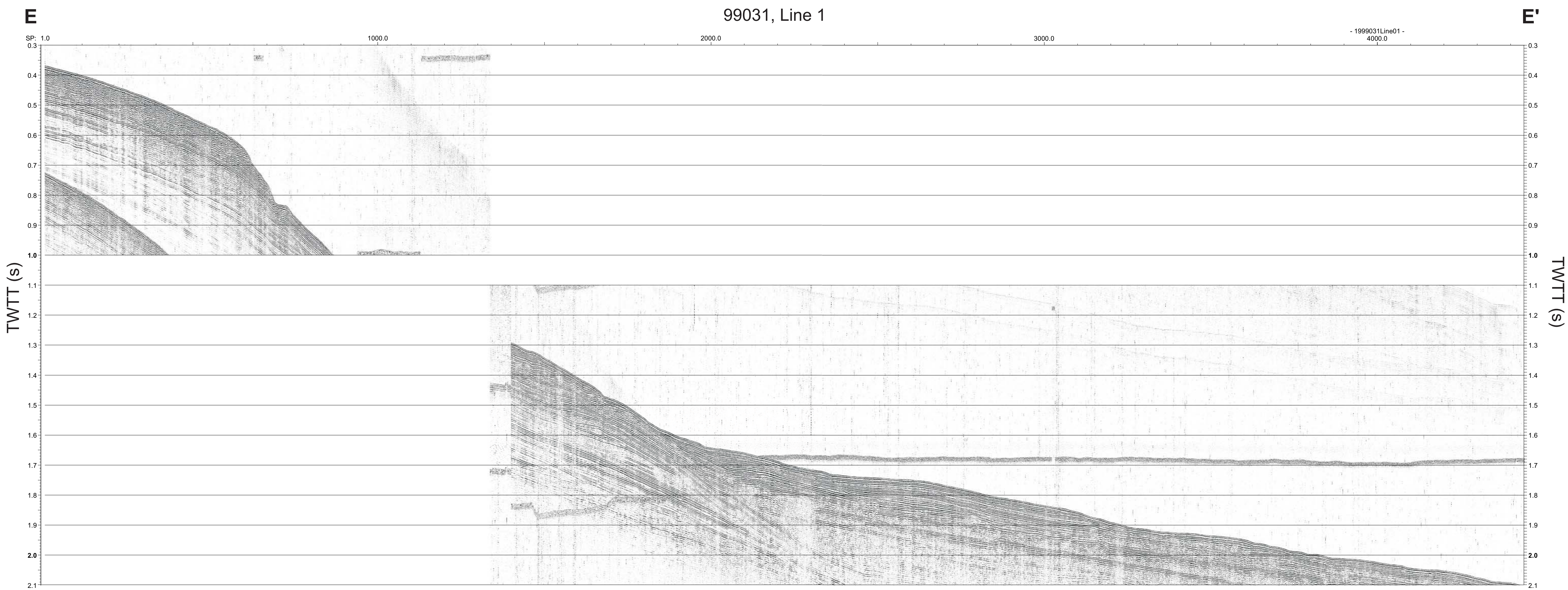
E
99031, Line 1
E'
SP: 1.0
1000.0
2000.0
3000.0
- 1999031Line01 -
4000.0
TWTT (s)
0.3
0.4
0.5
0.6
0.7
0.8
0.9
1.0
1.1
1.2
1.3
1.4
1.5
1.6
1.7
1.8
1.9
2.0
2.1
TWTT (s)